

Article

Prediction and Optimization Analysis of the Performance of an Office Building in an Extremely Hot and Cold Region

Yunbo Liu, Wanjiang Wang * and Yumeng Huang

College of Architectural and Civil Engineering, Xinjiang University, Urumqi 830017, China; 107552201577@stu.xju.edu.cn (Y.L.); 107552201606@stu.xju.edu.cn (Y.H.)

* Correspondence: wangwanjiang@xju.edu.cn

Abstract: The White Paper on Peak Carbon and Carbon Neutral Action 2022 states that China is to achieve peak carbon by 2030 and carbon neutrality by 2060. Based on the “3060 dual-carbon” goal, how to improve the efficiency of energy performance is an important prerequisite for building a low-carbon, energy-saving, green, and beautiful China. The office performance building studied in this paper is located in the urban area of Turpan, where the climate is characterized by an extremely hot summer environment and a cold winter environment. At the same time, the building is oriented east–west, with the main façade facing west, and the main façade consists of a large area of single-layer glass curtain wall, which is affected by western sunlight. As a result, there are serious problems with the building’s energy consumption, which in turn leads to excessive carbon emissions and high life cycle costs for the building. To address the above problems, this paper analyzes and optimizes the following four dimensions. First, the article creates a Convolutional Neural Network (CNN) prediction model with Total Energy Use in Buildings (TEUI), Global Warming Potential (GWP), and Life Cycle Costs (LCC) as the performance objectives. After optimization, the R^2 of the three are 0.9908, 0.9869, and 0.9969, respectively, thus solving the problem of low accuracy of traditional prediction models. Next, the NSGA-II algorithm is used to optimize the three performance objectives, which are reduced by 41.94%, 40.61%, and 31.29%, respectively. Then, in the program decision stage, this paper uses two empowered Topsis methods to optimize this building performance problem. Finally, the article analyzes the variables using two sensitivity analysis methods. Through the above research, this paper provides a framework of optimization ideas for office buildings in extremely hot and cold regions while focusing on the four major aspects of machine learning, multi-objective optimization, decision analysis, and sensitivity analysis systematically and completely. For the development of office buildings in the region, whether in the early program design or in the later stages, energy-saving measures to optimize the design have laid the foundation of important guidelines.

Keywords: convolutional neural network (CNN); NSGA-II algorithm; extremely hot and cold areas; office building performance optimization; sensitivity analysis



Citation: Liu, Y.; Wang, W.; Huang, Y. Prediction and Optimization Analysis of the Performance of an Office Building in an Extremely Hot and Cold Region. *Sustainability* **2024**, *16*, 4268. <https://doi.org/10.3390/su16104268>

Academic Editors: Igor Martek and Mehdi Amirkhani

Received: 3 April 2024

Revised: 3 May 2024

Accepted: 13 May 2024

Published: 18 May 2024



Copyright: © 2024 by the authors. Licensee MDPI, Basel, Switzerland. This article is an open access article distributed under the terms and conditions of the Creative Commons Attribution (CC BY) license (<https://creativecommons.org/licenses/by/4.0/>).

1. Introduction

The world today is undergoing a major change not seen in a century, and human society is facing unprecedented global challenges and changes. These challenges and changes come from a variety of sources, including the economy, the environment, and energy, and their impact is far-reaching, comprehensive, and long-lasting. Among other things, in terms of energy consumption, China already accounts for 15% of the world in terms of GDP levels. Regarding the level of energy consumption, China has accounted for 23.2% of the world’s total energy consumption and 33.6% of the world’s energy consumption growth rate. Building energy use accounts for a significant proportion of China’s energy consumption level. By the end of 2020, China’s buildings with high energy usage will reach 70 billion square meters, and the amount of energy consumed by buildings will be equal to 108.9 billion tons of standard coal. In addition, buildings have relatively long life cycles

with complex and dynamic behaviors. Therefore, more research is needed to incorporate building performance factors into building design standards. Under China's proposal to achieve a carbon peak by 2030 and carbon neutrality by 2060 (dual-carbon policy), it is especially important to know how to effectively save energy and reduce emissions at the office building level. The case studied in this paper is located in the city of Turpan, a region whose climate is characterized by hot summers, cold winters, extreme solar radiation, and annual precipitation of only 15 mm. As a result, there is an overconsumption of energy use in buildings, which also creates a series of problems in the built environment, e.g., excessive energy consumption in office buildings, excessive carbon emissions from buildings, high life cycle costs, and poor building thermal comfort, to name a few. Based on the above status quo, it is urgent to optimize how to improve these problems. At the same time, how to effectively optimize these issues is also in line with the concept of "Beautiful China" proposed by China in recent years. The so-called "Beautiful China" concept is to build a green civilization and integrate it into all aspects of cultural, economic, and social construction. It is specifically divided into two aspects: one is the establishment of a good ecological green environment, and the other is the implementation of low-carbon, green, and energy-saving forms of production and lifestyles. The measures proposed in this paper to optimize the performance of office buildings in Turpan fall into the category of green, energy-saving, and low-carbon production methods. At the same time, on the one hand, building performance optimization can guide the sustainable development of the construction industry, maximize the efficiency of energy use, and promote the effective implementation of energy-saving strategies. On the other hand, building performance optimization can drive change in human society, taking into account the energy–economy balance. Therefore, this paper conducts a performance optimization study for office buildings in Turpan to explore the climate adaptation law of office buildings in extremely hot and cold areas from the perspective of multiple performances, exploring practical optimization and design strategies applicable to local climate characteristics. This is of great practical significance for improving the energy consumption and economic costs of local office buildings, better tapping and inheriting the wisdom of construction, and even realizing China's "dual-carbon" target strategy. The article is divided into the following sections: The first part is the introduction to the article. The second part of the paper is a literature review. The third part is the methodology of the thesis, which includes various methods of analysis and the main framework of the thesis. The fourth part is a simulation study of the performance of office buildings in Turpan. The fifth part is a visual analysis of the results of predictive optimization of office building performance. The sixth part of the article is the discussion section of the paper. The seventh part is the conclusion of the paper and the coming outlook extension.

2. Literature Review

Currently, predictive optimization of office building performance focuses on energy consumption, economics, environmental impact, and thermal comfort. Specific detailing studies transition from building performance simulation to data-driven model creation, multi-objective optimization, sensitivity analysis, and more. In the following, we will analyze the research related to the optimization measures of office building performance prediction by scholars from different perspectives and in regard to several aspects.

2.1. At the Level of Building Energy Consumption

Building energy use has a profound impact on the performance issues of office buildings during their life cycle phases [1–17]. Several scholars have conducted relevant research on how to use effective energy saving and environmental protection optimization strategies to improve the energy performance of office buildings. Liu et al. studied the energy-saving strategies in terms of energy consumption in office buildings in Turpan. The article concludes that the west façade of the building, using double-glazed curtain wall circulation, combined with the east façade of the east-light south-oriented measures to reduce energy consumption, is the largest, affecting the program heating level by 64.14%, the cooling level

by 77.12%, and the total energy consumption level by 69.67% [1]. Valladares-Rendón et al. investigated the effect of overhangs on the energy performance of the building, as well as on the light performance, while studying the effect of overhangs. The results show that the use of the Overhanging Device-Single Edge Single Level (OD-SEL) system has great potential to reduce the energy consumption of building cooling [2]. Khabir et al. investigated the effect of energy consumption in office buildings by studying the double skin façade. The results show that a double skin façade with cooling materials can reduce energy consumption by 62–63% and a double skin façade with cooling materials can reduce CO₂ emissions by 76–77% [4]. Al-Tamimi scholars found a 26.81% reduction in total building energy consumption by studying different building envelope optimization strategies, such as changing the window glazing type and adding insulation [6]. Huo et al. investigated the effect of external blinds on the energy performance of office buildings. The article shows that, by changing different shading performance measures such as shading angle, window-to-wall ratio, and orientation, it is possible to improve the energy efficiency of buildings and reduce the energy consumption of office buildings [8]. Hashemi scholars studied the impact of automatic reflective blind systems on the energy performance of buildings by showing that the measure can save up to 60% of a building's energy consumption [10]. Cuce scholars investigated an insulated solar glass (HISG) technology. The results of the study showed that HISG can reduce building energy consumption by 38% and 48% during the heating and cooling seasons, respectively [15]. Ihara et al. explored the impact on building energy consumption by examining four characteristics related to energy efficiency in office buildings. The article shows that improving the SHGC and U-value of windows and increasing the solar reflectance of opaque parts can efficiently reduce building energy consumption [16].

2.2. At the Building GWP Level

At the level of carbon emissions from buildings, excessive carbon emissions can lead to a sharp increase in greenhouse gases and waste of energy resources, which in turn can lead to building environmental problems such as the heat island effect. The issue of how to effectively reduce carbon emissions is critical to improving building performance [18–35]. For example, the following scholars have conducted relevant studies: Zhang et al. investigated the impact of three objectives, GWP, global cost (GC), and operational energy (OE), on the ability to optimize building performance. The article found that the use of meta-model optimization resulted in a reduction of 12.7%, 6.7%, and 7.4% in the three metrics, respectively [22]. Yu et al. optimized the design process by establishing a parametric optimization to minimize GWP, energy consumption, and life cycle costs (LCCs). The results showed that optimizing all variables can achieve good building performance results [23]. Wang et al. examined the abatement potential of HFC emissions. The results indicated that the total GHG reduction capacity by 2050 is approximately equal to 10% of the total carbon emissions from the Chinese construction sector [24]. Honarvar et al. examined the evolution of buildings over their life cycle, and the results showed that the environmental impact of new materials increases fivefold in terms of GWP. Additionally, according to the circular economy concept, 10% of old and 3% of new housing materials can be returned to the chain, which in turn can reduce the GWP of the building during the life cycle [26]. Zhang et al. examined the effectiveness of buildings in reducing emissions during energy efficiency retrofits. The results show that retrofitting existing buildings can reduce considerable CO₂ equivalent and economic costs [27]. Wang et al. went on to improve environmental issues by examining building performance issues at life cycle costs. The results of the study showed that optimizing energy consumption, thermal comfort, and GWP using a multi-objective optimization algorithm can save the designer time and costs while reducing the range of alternatives [29]. Ansah et al. examined the impact of different façade materials on the environmental and economic costs of buildings in Ghana. The results show that stabilized earth block curtain wall is the most energy-efficient façade material with the highest potential for development, which can reduce GWP by 18.07% and

LCC by 47.87% [30]. Javid et al. studied the impact of energy consumption and GWP on buildings. In their paper, economic cost and GWP are used as the optimization objectives, and the results show that the use of optimization can lead to a reduction of 17.79% and 20.8% CO₂ equivalent for the two case buildings in the paper, respectively. In addition, buildings should be retrofitted from a life cycle perspective [32]. Hossain et al. studied the impact of building materials on GWP. The results showed that the construction of a 1 m hoarding produces three tons of CO₂ equivalent GWP [34]. Van Ooteghem et al. conducted a life cycle perspective to investigate which part of the building's structure would have the greatest impact on energy consumption and GWP. The results show that the building operation energy level is more influential, accounting for about 91% of the total energy consumption and 88% of the total GWP in terms of GWP [35].

2.3. At the Level of Building Life Cycle Costs

Incorporating buildings into the study of life cycle costs in turn improves building performance issues from the perspective of the whole-life economics of buildings [36–56]. The following scholars have studied how to make improvements at the LCC level: Lei et al. examined the application of green building design costs across the life cycle stages. The results showed that the cost of the operational phase of the building was the highest at 65.4% [36]. Kazem et al. went on to explore the effectiveness of energy efficiency retrofits in Cairo buildings through a whole-life-cycle cost analysis. The results showed that the most cost-effective façade retrofit was the installation of 1 m long external shading facilities, which reduced LCC by 1.4% and energy consumption by 18% [37]. Weerasinghe et al. went on to analyze the impact of green building costs in Sri Lanka by examining the life cycle costs of the building in its aspect. The results show that, although the initial construction cost of green buildings is 29% higher than that of conventional buildings, green buildings can save 23% and 15% of economic costs in the operation and maintenance phases, respectively, over their entire life cycle [39]. Yuan et al. examined how the performance of buildings changes by looking at energy savings and life cycle costs. The results showed that the 16 buildings corresponding to the use of the 16 envelope schemes met the green building evaluation criteria. At the same time, the article shows that life cycle costs rise as energy efficiency rates increase [43]. Xue et al. developed an LCA-LCC model by targeting building sustainability. The article's research found that economic costs were highest during the operational phase of the life cycle and that ADP-fossil and GWP metrics were most prominent throughout the life cycle [45]. Dwaikat et al. studied the application of life cycle cost in the construction industry. The article showed that the future costs of the studied buildings were 3.6 times their initial investment and construction costs, also showing that energy consumption accounts for 48% of the total life cycle costs and that reducing energy consumption reduces the total life cycle costs [47]. Schwartz et al. investigated the impact of buildings on energy use by taking a life cycle perspective, and the article optimized the LCC and Life Cycle Carbon Footprint (LCCF) through a multi-objective optimization genetic algorithm. The results showed that LCCF and LCC could be reduced by this method [49]. Invidiata et al. analyzed four shading systems that affected the energy performance of buildings by looking at them from a life cycle cost perspective. The results showed that the use of wooden double-opening blinds and PVC roller shades was the most appropriate window shading solution, efficiently reducing the building's energy consumption [50]. Abdallah et al. went on to reduce the life cycle cost of buildings by studying building optimization measures. The article proposed a model that identified the best building optimization measures and also significantly reduced the life cycle cost of a building [51]. Han et al. used numerical sensitivity analysis to understand the role of life cycle analysis (LCA) in building design. The results showed a significant correlation between energy modeling and life cycle costs. Also, wall assemblies had a much greater impact on life cycle costs than window performance [52]. Kneifel scholars have verified this by examining the effectiveness of new buildings in saving energy, reducing carbon, and lowering economic costs over their life cycles. Research results have shown that conventional technologies can

reduce the energy consumption of new buildings by 20–30%, while the carbon footprint can be reduced by 16% [55].

2.4. At the Level of Multi-Objective Optimization

The NSGA-II algorithm (a type of multi-objective optimization algorithm) uses a fast non-dominated sorting algorithm, which makes the computational complexity much lower than NSGA. At the same time, it introduces congestion and crowding operators that enable individuals in a quasi-Pareto domain to extend to the entire Pareto domain, ensuring population diversity. Finally, it introduces elite strategies that greatly increase the speed of computation in optimizing building performance metrics. Therefore, the method is widely used in the field of building performance optimization [57–63]. For example, the following scholars have performed relevant research in this area. Zhou et al. used a multi-objective optimization approach for building performance objective optimization, which in turn resulted in performance objective alternatives with optimal solutions [57]. Wang et al. performed a multi-objective optimization by targeting low energy consumption, better thermal comfort, and light performance. The results show that multi-objective optimization of the target indicators can reduce building energy consumption and improve energy efficiency [58]. Harkouss et al. present a method for simulating near-zero energy building (NZEB) optimization. The results show that the use of the NSGA-II algorithm can significantly reduce the thermal, electrical, and life cycle costs of buildings [63].

2.5. At the Machine Learning Level

The CNN deep neural network model is used to predict the building performance, and it can abolish problems such as the low prediction accuracy of traditional data-driven models. Meanwhile, CNNs with backpropagation algorithms can automatically adjust the network parameters to minimize the loss function, thus improving the performance of the network, i.e., it can enhance the predictive performance of buildings and minimize the time cost [64–77]. For example, the following scholars have conducted relevant studies at this level: Yue et al. investigated the application of data-driven modeling to building energy consumption and indoor environments by studying. Yue et al. investigated the impact of data-driven modeling on building performance through the application of data-driven models to building energy consumption and indoor environment. The results of the study showed that the use of data-driven models can greatly reduce the time cost, while, at the same time, the prediction results are more accurate [64]. Xu et al. went on to analyze issues such as improving the energy performance of buildings by studying building performance strategies. The results show that, by using the CNN data-driven model, building energy consumption can be optimized to reduce it by 24.53% [70]. Pal et al. went about predicting target metrics by employing a data-driven model using CNN combined with the NSGA-II algorithm. The results showed an accuracy of 94.83% and 94.96% on the two case datasets [73]. Bakar et al. attempted to optimize the target metrics by using a CNN combined with the NSGA-II algorithm, and the results showed that the CNN data-driven model has a better adaptive capability [77].

However, compared to the above literature studies, there are fewer studies on the building performance of office buildings throughout their life cycle in the cold regions of China. The Turpan region has increasingly hot summers and cold winters, and the maximum outdoor temperature in the Turpan region in 2023 reached 52.2 °C, the highest temperature recorded in China, indicating the relatively harsh environmental conditions in the region. In addition to this, after researching the office buildings in the region, it was found that several problems are common in the office buildings in the region, such as excessive building energy consumption, high carbon emissions from buildings, high building construction costs, and poor building thermal comfort. At the same time, office buildings in the region have relatively poor insulation and airtightness. A low-performing building envelope can cause a building to lose more heat in the winter. Poor airtightness increases the risk of cold air infiltration, which in turn leads to increased

energy consumption and running time of the heating equipment. In addition to this, office buildings in the region still face many dilemmas when it comes to optimizing them during their life cycle phases. For example, it is known from the research that local office buildings are reluctant to fund improvements in performance optimization due to the limitations of the local economic level and environmental awareness. Government makers are more focused on reducing greenhouse gas emissions, while office workers are more concerned with improving indoor comfort. Therefore, it is challenging to carry out office building performance optimization strategies in this region. However, elsewhere, several researchers have improved and optimized the above problem. For example, Luo et al. proposed a framework for whole-life optimization of building performance that takes climate change into account, it was implemented in two case buildings in the UK. The results show that the life cycle cost of a building was underestimated by 2.0–1.7% and the carbon emissions were underestimated by 1.2–6.9% when the optimized scenario decided in 2019 was adopted in the years between 2021 and 2024 [78]. Zhang et al. studied building performance in extremely dry and hot climatic conditions. That is, the effects of wall thermal resistance, roof thermal resistance, hole-to-wall area ratio, and wall interior height on the indoor environment were analyzed by numerical simulation, and the results of the study found that the hole-to-wall area ratio is the most important parameter affecting the indoor environment of life cycle buildings [79]. At the same time, in the study of office buildings in the Turpan region, it is necessary to further explore more optimized designs of office buildings so that the buildings in the region can adopt low-cost optimization strategies and have high performances in order to improve the comprehensive performance of the life cycle of office buildings in the region.

Based on the above analysis and research, the research of this paper is shown below: (1) Creating data-driven predictive models with high accuracy. Data-driven models represent a capability for fast analytical calculations with an accuracy close to that of dynamic simulations. They can be used as a strategy for conducting independent variable parameter studies and optimizing future building performance predictions. In this paper, eight data-driven models are selected to predict each of the three target indicators. (2) Multi-objective optimization is performed for three objective values. In this paper, the NSGA-II optimization algorithm is used to optimize the TEUI, GWP, and LCC, which leads to the results of the optimization scheme. (3) Decision analysis. In this part of the article, two Topsis methods are used to evaluate the performance optimization of office buildings. They are the entropy law form and the subjective empowerment form, respectively. There is use of multiple decision research methods for analysis, which in turn can increase the transparency of decision design. (4) Sensitivity analysis of variables. Two sensitivity analysis methods are used in this paper: the RBD-FAST method and the DMIM method. The article uses the method to visualize the variables analytically.

The main innovations of this paper are shown below:

- (1) In this paper, the CNN data-driven model is used to predict the performance target. Under the condition of guaranteeing accuracy, the target is realized to optimize quickly. Compared with the traditional prediction method, it improves the performance-driven design efficiency.
- (2) In this paper, the NSGA-II multi-objective optimization algorithm is used to quickly optimize the performance objectives, and the resulting optimization can provide ideas for builders in the area when performing building design.
- (3) The article provides an entropy-based decision-making method for Topsis. The method can help designers to make trade-off judgments in decision-making.

3. Methodology

3.1. BPS

Building Performance Simulation (BPS) is a powerful tool for studying the performance of a building's physical environment, and it can be used to achieve desired results with its easy hands-on capabilities. Therefore, it is increasingly used for research and

prediction of building energy consumption, measurement and verification, carbon emissions, and economic evaluation. It has played an indelible role in the design strategy of low-energy, high-performance office buildings and has been a good guide in promoting China's "dual-carbon" approach. In this paper, Rhion software (Rhino 7.0) is used for building performance simulation tools, and the GH plug-in that comes with the software can be easily used for office building performance simulation and analysis. Since the targets studied in this paper are TEUI, GWP, and LCC, the Rhion software and GH plug-in are divided as follows: In the office building energy consumption section, this article uses Ladybug Tools and the Honeybee plug-in. The Honeybee plug-in is embedded with the EnergyPlus energy calculation engine to facilitate the calculation of energy consumption. For carbon emission and life cycle cost calculations, this paper uses the Python module of the GH plug-in, which utilizes programming techniques that allow for quick analysis and calculations.

3.2. Machine Learning Neural Networks

When using physical models of building performance for analysis, traditional processes typically calibrate the model to match previous data through statistical inversion strategies. To reduce such errors between the model and the observed data, this matching process is time-consuming and costly, while, at the same time, most building performance simulation software is computationally intensive [80,81]. The resulting emergence of data-driven models can significantly reduce the cost of time. Data-driven modeling represents a form of fast execution of calculations with an accuracy close to that of dynamic simulation. It helps decision-makers to quickly examine high-dimensional performance simulations and immediately derive solutions under various constraints. Therefore, the deep learning model used in this paper can effectively solve the problem of high time cost. Currently, the commonly used learning algorithms in the field of building performance prediction and optimization are RNN, LSTM, and GAN, while CNN is less used in this field. CNNs are highly adaptable in terms of local feature capture performance. It can be used in the field of building performance by constructing high-dimensional features, which can effectively learn the relationship between the nonlinear interactions among the variables affecting TEUI, GWP, and LCC. In this paper, eight data-driven models are used to analyze and optimize building performance objectives; these eight data-driven models are Backpropagation network (BP), Support Vector Machine (SVM), Genetic algorithm-based optimized BP neural network (GA-BP), BP neural network based on particle swarm optimization algorithm (PSO-BP), SVM based on particle swarm optimization algorithm (PSO-SVM), CNN(SGDM) based on different optimizers, CNN(Adam) based on different optimizers, and CNN(RMSprop) based on different optimizers.

Among them, at the CNN level, CNNs can reduce the problem of too many model parameters due to excessive dimensionality by dealing with local correlations in the input data. The key feature of CNN operations is weight sharing [82]. When the convolutional kernel scans for local features in the data, the mechanism by which the convolutional kernel extracts the data after moving a certain number of steps remains unchanged. After the constant movement of the convolution kernel, the data scanning is completed and fewer parameters are obtained. CNNs generally include a convolutional layer, an activation layer, a pooling layer, and a fully connected layer. Convolutional layers extract information from foreign data and can be categorized as row-by-row and column-by-column, depending on the direction of scanning along the input features. Input features from all individual moment points are first combined by CNN line-by-line scanning. All combined features are then learned in a time series by transposing the input data into two dimensions when importing it into the training model, which in turn transitions to column-by-column scanning. This facilitates the convolution kernel to extract features from the data to form a feature mapping map, i.e., the convolution kernel operates by regularly sweeping through the input features, making matrix element multiplicative summations of the input features

within the receptive field and superimposing the amount of bias. The relevant equations are expressed below.

$$Z^{l+1}(i, j) = [Z^l \otimes w^{l+1}](i, j) + b = \sum_{k=1}^{K_l} \sum_{x=1}^f \sum_{y=1}^f [Z_k^l(s_0i + x, s_0j + y)]w_k^{l+1} \quad (1)$$

$$(i, j) \in \{0, 1, \dots, L_{l+1}\} \quad L_{l+1} = \frac{L_l + 2p - f}{s_0} + 1 \quad (2)$$

The summation part of Equation (1) is equivalent to solving a cross-correlation. b is the amount of deviation. Z^l and Z^{l+1} denote the convolutional input and output of layer $l + 1$. L_{l+1} is the size of Z_{l+1} . $Z(i, j)$ corresponds to the pixels of the feature map. K is the number of channels of the feature map. f , s_0 , and p are convolutional layer parameters corresponding to the convolutional kernel size, convolutional step size, and number of filled layers. A schematic diagram of the convolution operation is shown in Figure 1.

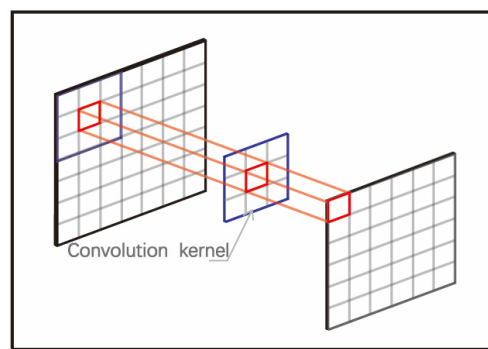
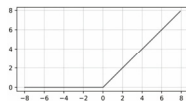
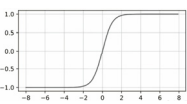
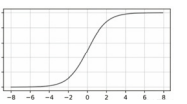
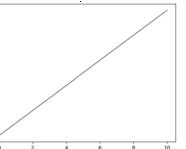


Figure 1. Schematic diagram of the convolution operation.

The feature is delivered through a nonlinear activation function that accelerates the CNN’s processing of complex relationships between data. Activation functions can generally be linear or nonlinear. The output of the former is simply a weighted sum of the inputs and cannot be backpropagated. While nonlinear functions have nonlinear functions, they can also solve linear functions. The activation functions routinely used are shown in Table 1. In this paper, the ReLU function is used.

Table 1. Activation functions in CNN data-driven models.

Function	ReLU	Tanh	Sigmoid	Linear
Formula	$y = \max(0, x)$	$y = \frac{1}{(1+e^{-x})}$	$y = \frac{e^x - e^{-x}}{e^x + e^{-x}}$	$y = ax$
Nature	Nonlinear	Nonlinear	Nonlinear	Linear
Range	$[0, \text{inf}]$	$[-1, 1]$	$[0, 1]$	$[-\text{inf}, \text{inf}]$
Response				

After feature extraction in the convolutional layer, the output feature map is passed to the pooling layer for feature selection and information filtering. The pooling layer contains predefined pooling functions whose function is to replace the result of a single point in the feature map with the feature map statistics of its neighboring regions. The pooling layer is inspired by the hierarchical structure within the visual cortex, which is generally represented by the model:

$$A_k^l(i, j) = \left[\sum_{x=1}^f \sum_{y=1}^f A_k^l(s_0i + x, s_0j + y)^p \right]^{\frac{1}{p}} \quad (3)$$

where the step size s_0 , and $\text{pixel}(i,j)$ have the same meaning as the convolutional layer. p is a pre-specified parameter. When p is equal to 1, it takes the mean value in the pooling region and is called mean pooling. When p tends to infinity, it takes an extreme value in the pooling region and is called extreme pooling. This paper is extremely pooled.

In addition, CNNs use optimizers that can change weights, learning rates, etc., to minimize the loss function. At the optimization level, the gradient descent method is the conventional method. In this, the gradient of the loss function for the parameters is operated and the parameters are updated by backpropagation on this basis. The parameter update equation is Equation (4).

$$\theta_{t+1} = \theta_t - \eta \mathbf{d}_t \quad (4)$$

where \mathbf{d}_t denotes the gradient of the objective function $J(\theta)$ based on the parameter θ at time t , and η represents the learning rate.

The difficulty of the gradient descent method is in the optimal value of the learning rate. Smaller learning rates require more training, while larger learning rates cause the network to converge quickly to a suboptimal solution.

Another aspect involves the adaptive learning rate methods. The most common are RMSprop and Adam. RMSprop can solve the difficulty of AdaGrad learning rate decay. The RMSprop weight update can divide the learning rate by the square root of the squared mean of the exponential decay gradient, $R[\mathbf{d}^2]_t$. The weight update formula is Equation (5).

$$\theta_{t+1} = \theta_t - \frac{\eta}{\sqrt{R[\mathbf{d}^2]_{t+\epsilon}}} \mathbf{d}_t \quad (5)$$

The Adam optimizer retains the exponentially decaying mean of the gradient squared and the exponentially decaying mean of the gradient.

The parameter-related calculation of the Adam optimizer is given in Equation (6).

$$\theta_{t+1} = \theta_t - \frac{\eta}{\sqrt{\hat{v}_{t+\epsilon}}} \hat{m}_t \quad (6)$$

where m_t and v_t represent the estimates of the first-order and second-order moments of the gradient, respectively. \hat{m}_t and \hat{v}_t represent the corrected m_t and v_t . The estimated first-order and second-order moments of the gradient are shown in the following table.

At the level of data-driven model evaluation, root mean square error (RMSE), mean absolute error (MAE), and coefficient of determination (R^2) are selected as the evaluation metrics of the results in this paper. Where R^2 shows the degree of deviation between the predicted and actual values of the model, the closer R^2 is to 1 (indicating that the direction between the predicted and actual values is more similar), the better the prediction effect. MAE and RMSE reflect the predictive accuracy of the data-driven model, with smaller values corresponding to a better predictive performance. Meanwhile, the various data-driven models analyzed in the article's study, as well as the construction of the various models, were analyzed and completed via Python (version 3.11) software.

$$RMSE = \sqrt{\frac{1}{n} \sum_{i=1}^n (\hat{y}_i - y_i)^2} \quad (7)$$

$$R^2 = 1 - \frac{\sum_i (\hat{y}_i - y_i)^2}{\sum_i (\bar{y}_i - y_i)^2} \quad (8)$$

$$MAE = \frac{1}{n} \sum_{i=1}^n |y_i - \hat{y}_i| \quad (9)$$

where y_i is expressed as the i actual value, \hat{y}_i is expressed as the i predicted value of the model, \bar{y}_i is the mean value, and n is the sample size of the data.

3.3. LHS

For data processing, this paper uses Latin Hypercube Sampling (LHS). It is a more advanced form of Monte Carlo sampling. It can divide the space of independent variable parameters into equal parts and then randomly sample on that basis. It effectively prevents aggregation of parameters and samples the entire space of variables. At the same time, the number of this sample is generally equal in number to about 5–15 times the number of parameters of the independent variable. At the level of data-driven model accuracy, to optimize its prediction performance, 2000 samples are taken for simulation in this paper to obtain the data set of the independent variable—the target variable. The specific procedure for Latin Hypercube Sampling (LHS) is as follows:

- (1) The sample size M of the independent variable and the number of dimensions m are established first.
- (2) Equalize the interval of the independent variable parameter X as $[lb, ub]$. That is, it is the maximum and minimum values of the parameters of the independent variables.
- (3) The interval of the independent variable parameter X is transformed into a homogeneous region of M equal parts.
- (4) Selection point samples were performed in each interval of each dimension.
- (5) All the points of the interval are added together to form a vector.

3.4. MOP Algorithm

In this paper, the NSGA-II algorithm is used for multi-objective optimization of objective values (TEUI, GWP, and LCC). The algorithm is a fast non-dominated solution MOP algorithm with an elite reservation mechanism [83]. Its superior performance characteristics have been widely used in various building industry designs and green building performance evaluations. In this paper, the population size and maximum number of generations were set to 45 and 100, and the probability of variation and crossover rate were set to 0.07 and 0.90. The optimization criterion is to minimize the TEUI, GWP, and LCC objective values by adjusting the parameters of the independent variables. Its expression is:

$$F(\vec{x}) = \begin{cases} f_1 = f(\vec{x}, TEUI)_{\min} \\ f_2 = f(\vec{x}, GWP)_{\min} \\ f_3 = f(\vec{x}, LCC)_{\min} \end{cases} \quad (10)$$

3.5. Decision Analysis

In the decision analysis section, this paper uses the entropy-based Topsis method [84–93] when making decisions on the optimization scheme. The method has the following advantages: The entropy weighting method can confirm the weighting information of the target indicators by analyzing the entropy value of the target indicators of each scenario, which in turn can provide a reference for the multi-objective assessment later. Topsis analysis uses matrix extrapolation to calculate the worst and optimal solutions and then derives the distance between the objective and the first two. Finally, the closeness of each target solution to the first two ideal solutions is derived. If the indicator is close to the positive ideal solution and far from the negative ideal solution, the result is good. Finally, the above two methods are fused into one, with the entropy weighting method being used to calculate the weights and the Topsis method being used for ranking. The specific practices are as follows:

- (1) Establishment of the matrix.
Use the initial data to build the matrix for m indicators and n objects.
- (2) Calculate the entropy value of the target variable.

According to the importance of each indicator to the comprehensive evaluation, the information entropy is used to calculate each entropy value.

$$e_j = \frac{-1}{\ln m \sum_{i=1}^m p_{ij} \ln p_{ij}} \quad (11)$$

- (3) The coefficient of variation in the target variable was established.
Let g_j be the coefficient of variation of target indicator j .

$$g_j = 1 - e_j \quad (12)$$

- (4) Determination of entropy weights of target indicators.

Let H_j be the entropy weight of target indicator j . Normalize g_j to obtain the indicator H_j .

$$H_j = \frac{g_j}{n} - \sum_{i=1}^n d_j \quad (13)$$

- (5) Analyze the distance between the result and the two ideal solutions.

$$Di^+ = \sqrt{\sum_{j=1}^n (z_{ij} - z_j^+)^2} \quad (14)$$

$$Di^- = \sqrt{\sum_{j=1}^n (z_{ij} - z_j^-)^2} \quad (15)$$

where Di^+ and Di^- denote the distance of the i evaluation object from the optimal and worst solutions, respectively.

- (6) Calculation of relative progress for each target indicator.

$$C_i = \frac{Di^-}{Di^+ + Di^-} \quad (16)$$

where C_i denotes the final score for each scenario. The value is $0 \leq C_i \leq 1$.

3.6. Sensitivity Analysis

Sensitivity analysis refers to the change in the outcome of the target variable, as the independent variable changes when a variable is varied within a certain range. Since sensitivity analysis can respond to the degree of influence of characteristic parameters on the performance of office buildings, it plays an important role in green building performance analysis, retrofitting of existing office buildings, and evaluation of building performance models. Two sensitivity analysis methods are used in this paper: RED-FAST and DMIM analytical methods. The DMIM method is a density-based global analysis method with proven authority at the methodological level of sensitivity analysis [94]. It has two types of visualization of analysis results when results are analyzed on the independent variable–target variable data set, TOI and FOI. FOI indicates the contribution of a single independent variable parameter to the output results. TOI indicates the contribution of a single independent variable and the interaction of that variable with other variables to the output result. The RBD-FAST method introduces the RBD concept at the level of the FAST method and then goes on to solve the shortcomings of the FAST method, which has too many sample points and too many time costs. At the same time, it is a complementary FOI to DMIM [95].

3.7. Research Framework for the Thesis

The full frame content of this paper is presented in Figure 2.

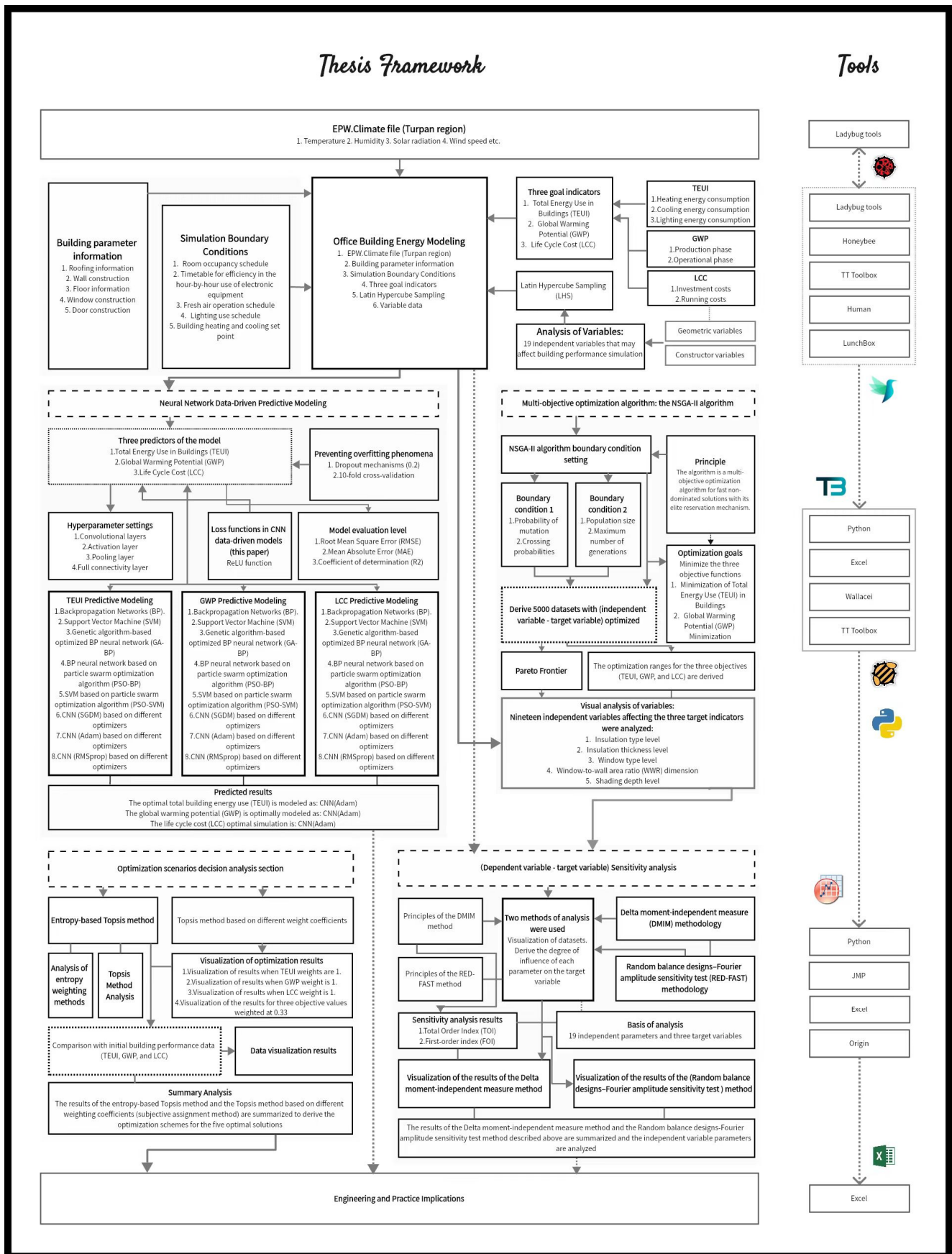


Figure 2. Article Framework Diagram.

Brief analysis: The content of the research framework of this paper is divided into the following sections. The first is building performance simulation. The independent-target variables were brought into the Rhion software to derive TEUI, GWP, and LCC. This involves bringing in the building envelope, the transparent envelope, and some other boundary conditions. The dataset was collected based on Latin Hypercube Sampling (LHS). Next, CNN data-driven model prediction, multi-objective optimization, decision analysis, and sensitivity analysis are performed based on building performance objectives (TEUI, GWP, and LCC), respectively. At the data-driven model prediction level, the article uses eight different prediction models to predict the three target values. In the multi-objective optimization phase, the article uses the NSGA-II algorithm to optimize the three objectives. In the decision analysis section, the article uses the entropy-based Topsis method and subjective empowerment to analyze the objectives. Finally, a sensitivity analysis of the variables was conducted using two methods.

4. Building Performance Simulation

4.1. Climate Analysis

The building site studied in this paper is located in the Turpan area of the Xinjiang Uygur Autonomous Region. The region is located in the eastern part of the Tien Shan Mountains and is shaped like an oval-shaped basin. It is surrounded by high mountains. The climate of the region is a continental warm temperate desert climate. In the thermal division of China, Turpan is located in the cold region. The region has hot, dry, and windy summers and cold winters. The total area of the Turpan region is 69,000 km² and the annual evaporation is 3100 mm, but the precipitation is only 15 mm. Temperature-wise, the area is over 37 °C for one-third of the year. Temperature extremes reach 52.2 °C in summer and −28 °C in winter. At the same time, the region is characterized by strong solar radiation, with an average daily total solar radiation rate of 16 KJ. At the level of data selection, this paper selects the CSWD literature climate data information of the Turpan area. CSWD meteorological data sources are compiled by the China Meteorological Administration (CMA), which are more in line with the meteorological data used for building design in China. These data are visualized in this paper by Ladybug Tools for climate data. Figure 3 represents typical meteorological annual radiation data for Turpan Point. Figure 4 represents additional data.

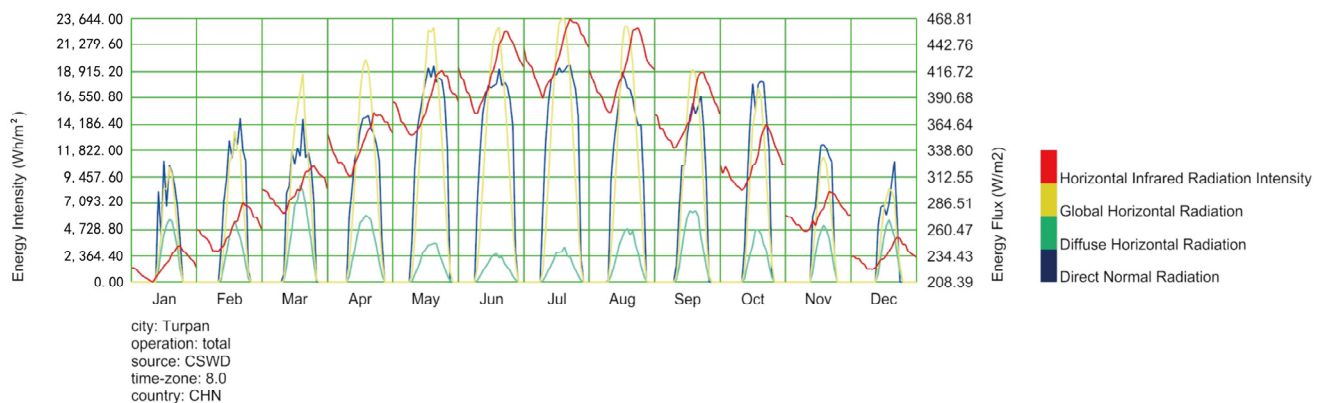


Figure 3. Climatological data for Turpan (radiation component).

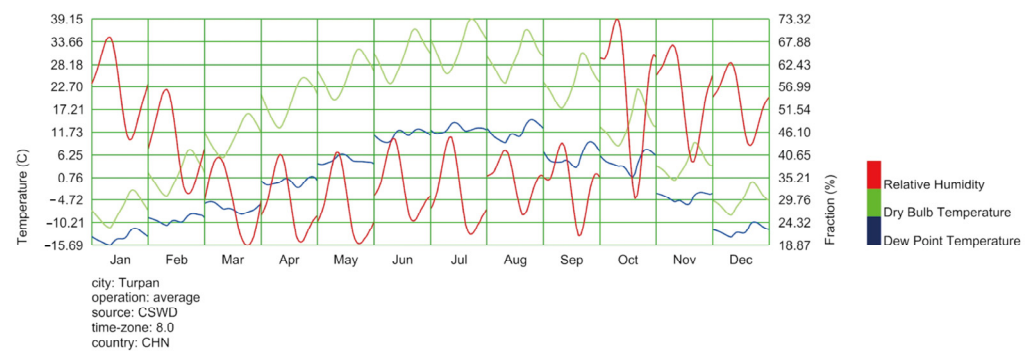


Figure 4. Climatological data for Turpan (other parts).

4.2. Office Building Case Presentations

In terms of location selection, the office building case selected in this paper is located in Turpan City. The building area is 4966 m², the number of floors is five, the height above ground is 32 m, the length is 62 m, and the width is 18 m. The building blocks are oriented east–west, with the main façade facing west, and the whole is symmetrical on the central axis. The façade of the building is in the form of a single-story glass curtain wall construction, with no snap caps on the surface of the glass curtain wall. There is a 13 m long, 4.5 m wide awning at the foyer. The east elevation of the building is framed by 70 mesh windows. The north and south elevations of the building are strips of glass curtain walls intended to provide light to the corridors. Figure 5 shows the office building portraits and models. Figure 6 shows the standard floor plan of the office building.

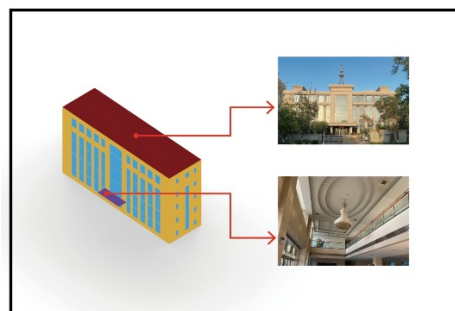


Figure 5. Office building portraits and model drawings.

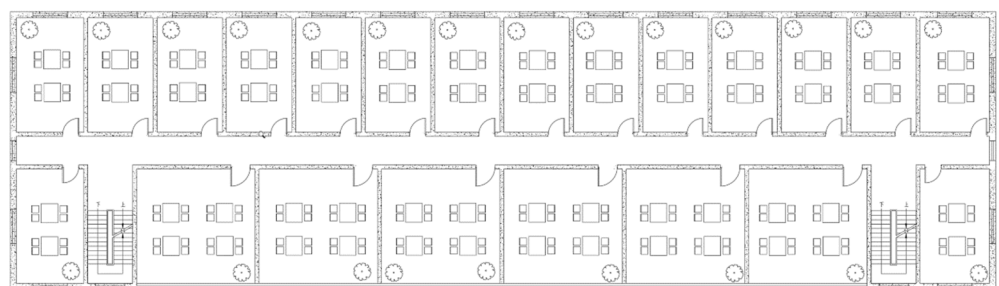


Figure 6. Building plan illustration.

4.3. Parameter Selection

Parametric modeling is an approach that makes use of geometric attribute variables. It enables designers to use mathematical and programming techniques to assemble to numerical models [96]. In this paper, in terms of parameter selection, 19 parameter variables that may affect the TEUI, GWP, and LCC of office buildings in Turpan are selected. It contains five building construction variables as well as 14 building geometry variables.

The type of exterior wall insulation (WIT), the type of roof insulation (RIT), and the type of windows (WT) are used as office building construction variables in this paper. According to the research, the commonly used insulation materials in the region are Expanded Polystyrene (EPS), Extruded Polystyrene (XPS), and Polyurethane (PU) boards, among others. Therefore, this paper selects the external insulation material aspects for the above three. At the window perspective level, this paper selects five types of external windows with different thermal properties, which are ranked as follows according to the level of performance, as shown in Table 2. In terms of architectural geometric variables, this paper includes five types: they are window-to-wall area ratio (WWR_N, WWR_E, WWR_S, WWR_W), shading system louver length (DEP_N, DEP_E, DEP_S, DEP_W), number of shading system louvers (Shade count_N, Shade count_E, Shade count_S, Shade count_W), shading angle of the east and west wall louvers of the shading system (Angle_E, Angle_W), thickness of the exterior wall insulation (TW), and thickness of roof insulation (TR), as shown in Table 3. In contrast to other conventional research analyses, this study considers the heat transfer process in different dimensions of the facade and the roof. At the same time, careful differentiation of the thickness of insulation between the two types of external walls and roofs can lead to finer optimization of energy saving and carbon reduction. Meanwhile, vertical and horizontal louvers are used for east–west and north–south directions, respectively. Defining the length and number of shading systems can be explored to study the extent to which exterior building shading systems affect the performance of office buildings in the Turpan region.

Table 2. Thermal performance data for office building materials.

Categories	Names	No.	Conductivity [W/(m·K)]	Specific Heat Capacity [J/kg·K]
Insulation	EPS	0	0.037	1380
	XPS	1	0.030	1380
	PU	2	0.024	1380
Categories	Names	No.	Conductivity [W/(m·K)]	SHGC
Window	Double pane, Low-e	0	2.1	0.6
	Double pane, Low-e, argon	1	1.7	0.6
	Triple pane, Low-e	2	1.3	0.55
	Triple pane, Low-e(green)	3	0.9	0.5

Table 3. Distribution data for 19 variables.

No.	Categories	Symbol	Unit	Range
1	Wall insulation type	WIT	/	[0–2]
2	Roof insulation type	RIT	/	[0–2]
3	Window type	WT	/	[0–3]
4	Window-to-wall ratio of north wall	WWR_N	/	[0–0.6]
5	Window-to-wall ratio of east wall	WWR_E	/	[0–0.6]
6	Window-to-wall ratio of south wall	WWR_S	/	[0–0.6]
7	Window-to-wall ratio of west wall	WWR_W	/	[0–0.6]
8	North-facing louver depth	DEP_N	m	[0–1.5]
9	East-facing louver depth	DEP_E	m	[0–1.5]
10	South-facing louver depth	DEP_S	m	[0–1.5]
11	West-facing louver depth	DEP_W	m	[0–1.5]
12	Number of north-facing louvers	SC_N	/	[0–5]
13	Number of East-facing louvers	SC_E	/	[0–5]
14	Number of South-facing louvers	SC_S	/	[0–5]
15	Number of West-facing louvers	SC_W	/	[0–5]
16	East-facing louver shading angle	A_E	(°)	[0–90]
17	West-facing louver shading angle	A_W	(°)	[0–90]
18	Wall insulation thickness	TW	mm	[0–330]
19	Roof insulation thickness	TR	mm	[0–330]

4.4. Research Indicators

4.4.1. TEUI

Energy consumption is the energy consumed during the use of a building. This includes energy consumption at the building heating level, cooling level, lighting level, and equipment level. Since office buildings are fundamentally different from residential buildings in terms of use functions, their total energy consumption is much greater than the latter. The building energy consumption studied in this paper is the sum of heating energy consumption per unit area (HEUI), cooling energy consumption per unit area (CEUI), and lighting energy consumption per unit area (LEUI). Combined, these are the total energy use per unit area (TEUI). The TEUI expression is:

$$E_{total} = \frac{E_{heat} + E_{cool} + E_{light}}{A_1} \quad (17)$$

where E_{total} —Total building energy consumption (kWh/m²); E_{heat} —Building heating energy consumption (kWh/m²); E_{cool} —Building cooling energy consumption (kWh/m²); E_{light} —Energy consumption of building lighting (kWh/m²); A_1 —Office floor space (m²).

4.4.2. GWP

In this paper, GWP is selected as an environmental indicator for office building performance evaluation. It can be used to screen the heat storage capacity of other gases in the atmosphere, such as CO₂, in terms of CO₂ equivalent. Therefore, this indicator was selected as the target indicator, representing the impact on the environment. In this paper, the calculation part of this GWP consists of two parts: carbon emissions during the production phase of building materials and the operational phase of the building. The formula is as follows, and the method used is the CEF calculation method. Table 4 represents the relevant parameter variables' economic costs and carbon emission factors.

$$GWP = \sum_{m=1}^M Q_m \times f_m + a \times \left[\frac{Q_H \cdot H}{\eta_H} \cdot f_c + \left(\frac{Q_c}{\eta_c} + E_L \right) \cdot f_e \right] \quad (18)$$

where m —type of construction material; Q_m —Quality of construction materials; f_m —CEF for construction materials; f_c —CEF for coal energy; f_e —CEF for electrical energy; a —The number of years of the survey, which is 50 years in this study.

Table 4. Construction material prices and carbon emission factor data.

Categories	Names	No.	Cost	CEF
Insulation	EPS	0	360 CNY/m ³	5.7 kgCO ₂ /kg
	XPS	1	450 CNY/m ³	20.1 kgCO ₂ /kg
	PU	2	1050 CNY/m ³	5.1 kgCO ₂ /kg
Window	Double pane, Low-e	0	340 CNY/m ²	92 kgCO ₂ /m ²
	Double pane, Low-e, argon	1	430 CNY/m ²	101 kgCO ₂ /m ²
	Triple pane, Low-e	2	620 CNY/m ²	130 kgCO ₂ /m ²
Energy	Triple pane, Low-e (green)	3	740 CNY/m ²	141 kgCO ₂ /m ²
	Coal	\	0.45 CNY/kg	2.62 kg/kg
	Electricity	\	0.48 CNY/kWh	0.89 kg/kWh

4.4.3. LCC

The life cycle cost is selected as the sum of the economic costs of the initial investment phase of the building and the operational phase of the building (LCC). It includes the economic cost of running the office building and the initial investment cost. It is the sum of the cost values over the entire life cycle. The life cycle for this study was chosen

to be 50 years, and only the initial construction and annual energy economic costs were considered for their impact on life cycle costs. The relevant formulas are as follows:

$$LCC = \frac{DLC + \sum_{i=1}^{50} [EC \cdot R_d(i)]}{A_{\text{floor}}} \quad (19)$$

$$R_d(i) = \frac{1 - (1 + R_r)^{-i}}{R_r} \quad (20)$$

$$R_r = \frac{R_i - R_e}{1 + R_e} \quad (21)$$

where LCC —Total Life Cycle Cost of Office Buildings; DLC —Difference in investment costs between the optimized building case and the reference building case (CNY); including the increased economic cost of the passive technology compared to the initial building; EC —Energy cost (CNY) in year i ; A_{floor} —Gross floor area of office buildings (m^2); $R_d(i)$ —Discount rate for year i ; R_r —Real Rate of Interest; R_e —Rate of escalation of costs, = 1.2%; R_i —market interest rate; = 4.25%. It is assumed that this energy demand remains constant over the number of years calculated.

Where EC is the economic cost of energy for the year. The formula is as follows:

$$EC = \frac{Q_H \cdot H}{\eta_H} \cdot P_H + \left(\frac{Q_c}{\eta_c} + E_L \right) \cdot P_E \quad (22)$$

where H —Electricity and coal conversion factor (kg/kWh); η_H —Heating efficiency, =0.82; P_H —Local area coal prices (CNY/kg); η_c —Cooling efficiency, =3; P_E —Price of Electricity (CNY/kWh).

4.5. Office Building Performance Simulation Modeling

4.5.1. Boundary Condition Setting

Office building performance model creation: For the Turpan office building studied in this paper, the thermal performance information of the relevant building materials and the carbon emission-related indexes are brought into the GH and Honeybee plug-ins during the creation of the performance model to provide the building envelope and transparent envelope performance information. At the same time, the geometric information required to create an office building is created via the Rhion software. The two are then blended into one in Ladybug Tools. Meanwhile, this paper samples the parameters of the independent variables using the LHS method, which is a commonly used sampling method in deep neural network model prediction. It avoids the problem of overlapping samples. Among them, in terms of the original office building performance data, this paper sets the thermal performance of the enclosure structure in the cold region of Turpan by the General Specification for the “General Specification for Energy Efficiency and Renewable Energy Utilization in Buildings” (GB55015-2021 [97]). From the field study, the office building has a body shape factor of 0.21. In terms of thermal parameters of building models, the K -value of the building’s exterior walls is $2.65 \text{ W}/(\text{m}^2 \cdot \text{K})$. The K -value of the roof is $0.88 \text{ W}/(\text{m}^2 \cdot \text{K})$, and the K -value of the exterior windows is $2.70 \text{ W}/(\text{m}^2 \cdot \text{K})$, with a SHGC of 0.30. This results in an initial TEUI of $258.76 \text{ kWh}/\text{m}^2$, a GWP of $116.51 \text{ kg}/\text{m}^2$, and an LCC of $270,192.01 \text{ CNY}/\text{m}^2$ for the office building (baseline model).

Aspects of setting operational parameters for office buildings: In terms of the building’s energy consumption, heating temperatures, cooling temperatures, and human activity affect the results. The building performance model studied in this paper refers to the General Specification for the “General Specification for Energy Efficiency and Renewable Energy Utilization in Buildings” (GB55015-2021) (hereinafter collectively referred to as the Specification). At the level of personnel activity rate influencing factors, the personnel presence rate, number of personnel, and personnel category all have important influencing effects on the TEUI, GWP, and LCC of this office building. The building’s personnel density

is set at 10 m²/person according to the code. Personnel in the room rate by the norms of the basis and then combined with the specific local work and rest time in the Turpan set, as shown in Figure 6. The room rate of personnel in the room is set accordingly with the specific local work and rest time in Turpan based on compliance with the specification, as shown in Figure 7. The cooling and heating temperatures in this paper are set concerning the temperatures in the code and combination with the local climatic characteristics of Turpan. In this paper, the indoor cooling temperature is set to 28 °C and the heating temperature is set to 18 °C. Cooling and heating schedules are set according to local working hours. The electrical equipment parameters are set at 15 W/m² according to the specifications. The hour-by-hour usage schedule of electrical equipment, the lighting usage schedule, and the building fresh air operation schedule are set in conjunction with specific local working hours, as shown in Figure 7.

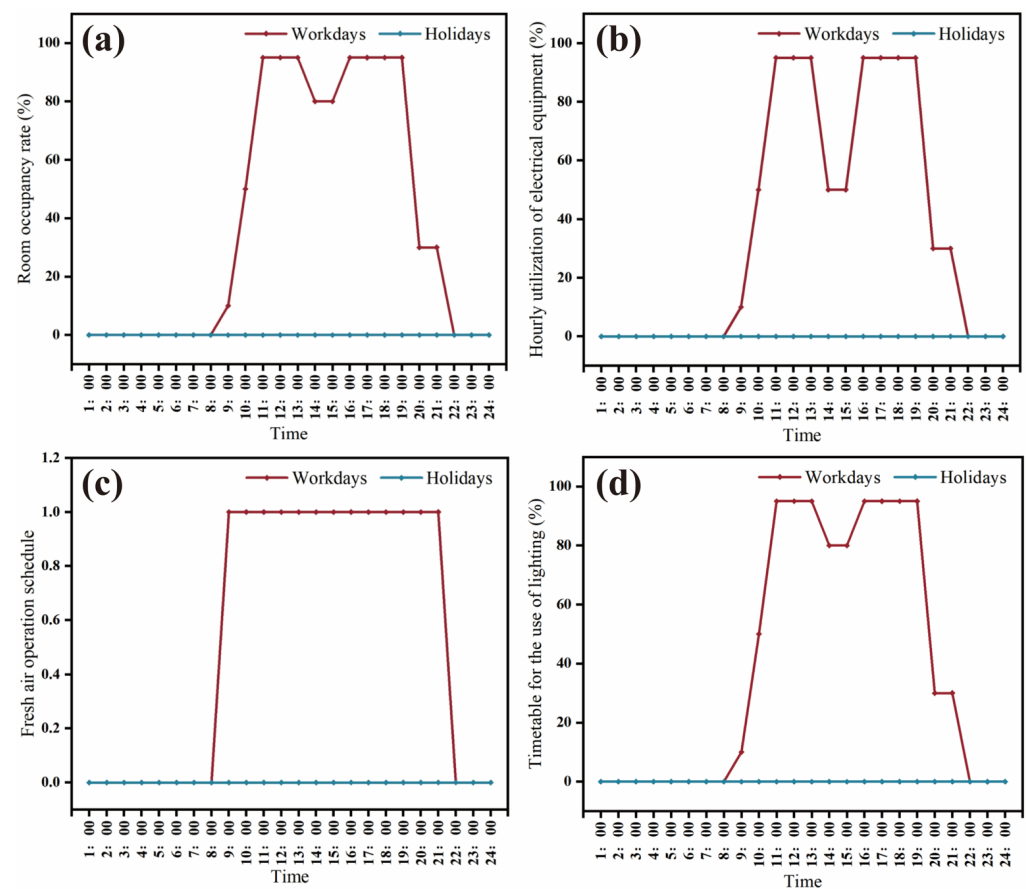


Figure 7. Building operating boundary condition settings. (a) Timetable of indoor occupancy rates. (b) Timetable for efficiency in the use of building equipment. (c) Building ventilation operating schedule. (d) Timetable for the use of lighting.

4.5.2. Other Condition Settings

Building performance data organization. In this paper, the Calibri Aggregator plug-in was chosen to statistically organize the building performance indicators (TEUI, GWP, and LCC). In addition, two widgets were connected to it: *CP Plugin*—which was mainly used as a target indicator for statistical building performance—and *CI Plugin*—which was mainly used to link the required samples. Finally, the Folder plug-in was used to save the records of the three target metrics of the building (TEUI, GWP, and LCC) to the Computer Specific Information folder. The target metrics obtained above are collected and organized and finally read into the xlsx file format for next use and analysis.

4.6. Building Performance Prediction Model Boundary Setting

After performing the independent variable-target variable dataset creation, this paper samples 2000 samples. An amount of 80% of these samples are used to train the model, and a 20% sample size is used to validate the accuracy of the model. The model consists of 19 input values (independent variable parameters) and three target values (TEUI, GWP, and LCC) with data of numerical type. After carrying out the prediction modeling, the selection of hyperparameters is also a difficult part of building a high-precision prediction model. In Deep Learning Convolutional Neural Networks (CNNs), the 2000 sample set is divided into 80% and 20% training and validation sets. To prevent the emergence of model overfitting risk, K-fold cross-validation is used in this paper for suppression. It can make the training set obtain more information and ensure the stability of the deep learning model. At the same time, outliers need to be culled. Outliers in the data that are not dealt with have no real meaning in the simulation, even though a deep learning model with higher accuracy can be obtained in the end. Therefore, the above method is used to establish a high-precision data-driven model with practical significance.

5. Results

5.1. Model Creation

Convolutional Neural Network (CNN) model creation. In this paper, three optimizers are chosen to change the weights, namely Adam, Sgdm, and RMSprop. The batch size for each model is 128. For the learning rate setting, the initial value is set to 0.01 in this paper. The input data are also standardized according to the standardization formula to eliminate the effect of the scale between the data. Meanwhile, to prevent the CNN data-driven model from encountering the overfitting phenomenon, this paper adopts the Dropout mechanism and K-fold cross-validation. The Dropout mechanism indicates that each neuron has a certain probability of being dropped, i.e., its output is 0 and the weights are not updated. In this paper, the Dropout value is set to 0.2, i.e., it means that 20% of randomly selected nodes will not be trained. Meanwhile, 7-fold cross-validation is used to improve the stability of deep learning models.

5.2. CNN Hyperparameter Settings

In CNN deep neural network models, more CNN layers lead to greater feature loss because the independent variable-target variable dataset is itself highly expressive. Therefore, this paper uses three layers for prediction. Meanwhile, the size of the convolution kernel in this paper is set to 3×3 , and the step size of each move of the convolution kernel is 1. The information about the hyperparameter settings of the CNN deep neural network in this paper is shown in Table 5.

Table 5. Visualization of CNN Convolutional and Pooling Layer Settings.

Layer	Filter Size	Pool Size	No.of Filters	Stride	Padding Strategy	Activation Functions
Conv-1	3×3	---	32	1	0	ReLU
Pool-1	---	2×2	---	2	---	---
Conv-2	3×3	---	64	1	0	ReLU
Pool-2	---	2×2	---	2	---	---
Conv-3	3×3	---	128	1	0	ReLU
Pool-3	---	2×2	---	2	---	---

5.3. TEUI Forecasting Model Analysis

The training process of the TEUI convolutional neural network model for the Turpan office building is shown in Figure 8.

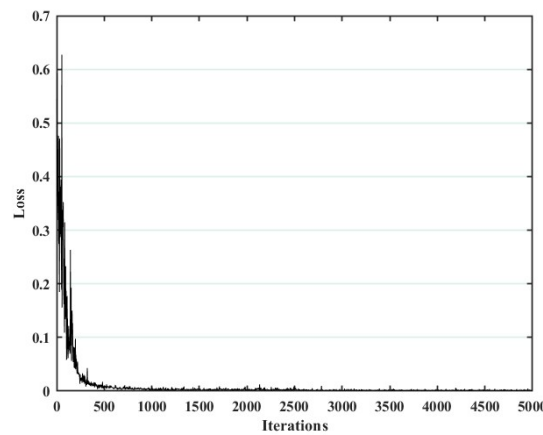


Figure 8. The CNN model training process for TEUI.

Analysis: In the case of the office building TEUI, the data information for the eight-building performance data-driven models is shown in Table 6. Also, the visualization results of R^2 , RMSE, and MAE are shown in Figure 9. It is found through the figure that, among the eight models, the CNN(Adam) model has the highest correlation coefficient and the lowest RMSE and MAE. At the same time, other evaluation models have shown some advantages. The building performance modeling accuracy (R^2) sizes are in the following order: CNN(Adam), GA-BP, PSO-BP, BP, PSO-SVM, CNN(RMSprop), CNN(Sgdm), SVM. Meanwhile, the order of size in terms of RMSE evaluation metrics is as follows: CNN(Adam), PSO-BP, GA-BP, BP, PSO-SVM, CNN(RMSprop), CNN(Sgdm), SVM. Additionally, the order of magnitude in terms of MAE evaluation metrics: CNN(Adam), GA-BP, PSO-BP, BP, CNN(RMSprop), CNN(Sgdm), SVM, PSO-SVM.

Table 6. TEUI data-driven model accuracy visualization results.

Sort	Model	RMSE	MAE	R^2
1	BP	0.2522	0.1917	0.9733
2	SVM	0.9272	0.8880	0.9361
3	GA-BP	0.1986	0.1354	0.9889
4	PSO-BP	0.1963	0.1503	0.9870
5	PSO-SVM	0.2964	0.9671	0.9699
6	CNN(Sgdm)	0.4082	0.2997	0.9408
7	CNN(Adam)	0.1871	0.1254	0.9908
8	CNN(RMSprop)	0.3170	0.2541	0.9628

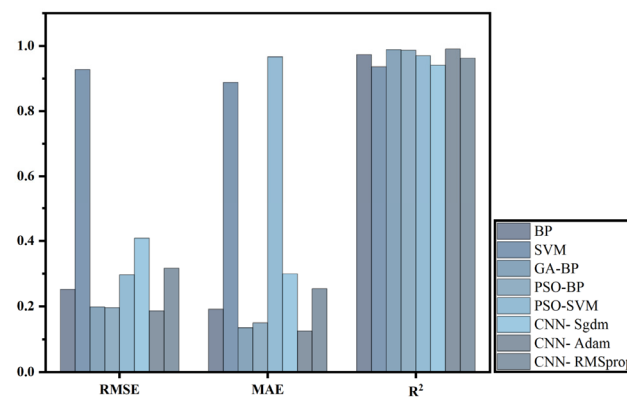


Figure 9. TEUI data-driven model accuracy visualization results.

In terms of deep learning models versus traditional regression models, CNN(Adam) reduces 0.0651, 0.7401, 0.0115, 0.0092, and 0.1093 in terms of RMSE compared to BP, SVM, GA-BP, PSO-BP, and PSO-SVM, respectively. MAE decreased by 0.0663, 0.7626, 0.01, 0.0249, and 0.8417, respectively. As for R^2 , CNN(Adam) ranked the highest. The above analytical study shows that the CNN(Adam) algorithm outperforms all other data-driven models in predicting the error of the network prediction model concerning the data. It has the highest R^2 score and the smallest RMSE and MAE values. This means that CNN(Adam) can be better generalized to new sample data and can be effectively used to predict data for architectural TEUI.

5.4. GWP Prediction Model Visualization Results

The training process of the GWP convolutional neural network model of the Turpan office building is shown in Figure 10.

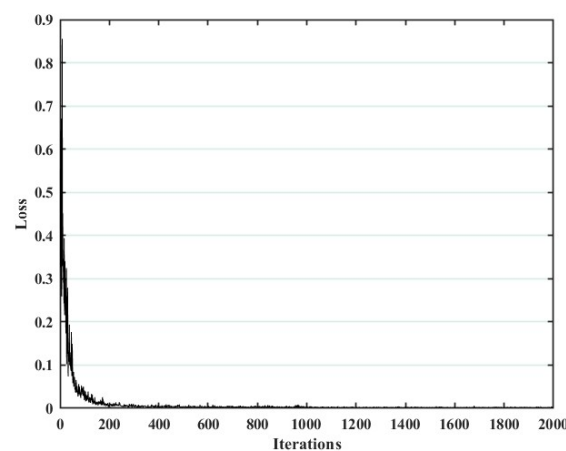


Figure 10. The CNN model training process for GWP.

Analysis: In terms of office building GWP, the data information for the eight-building performance data-driven models is shown in Table 7. Also, the visualization results of R^2 , RMSE, and MAE are shown in Figure 11. It is found through the figure that, among the eight models, the CNN(Adam) model has the highest correlation coefficient and the lowest RMSE and MAE. At the same time, other evaluation models have shown some advantages. The building performance modeling accuracy (R^2) sizes are in the following order: CNN(Adam), PSO-BP, PSO-SVM, CNN(RMSprop), GA-BP, BP, CNN(Sgdm), SVM. Additionally, the order of size in terms of RMSE evaluation metrics is as follows: CNN(Adam), CNN(RMSprop), GA-BP, PSO-SVM, BP, CNN(Sgdm), SVM, PSO-BP. Finally, the order of magnitude in terms of MAE evaluation metrics is as follows: CNN(Adam), BP, CNN(Sgdm), CNN(RMSprop), SVM, PSO-BP, PSO-SVM, GA-BP.

Table 7. GWP data-driven model accuracy visualization results.

Sort	Model	RMSE	MAE	R^2
1	BP	0.1817	0.1501	0.9485
2	SVM	0.4141	0.4013	0.9029
3	GA-BP	0.1325	0.9471	0.9727
4	PSO-BP	0.8934	0.6774	0.9818
5	PSO-SVM	0.1447	0.7568	0.9797
6	CNN(Sgdm)	0.1966	0.1512	0.9436
7	CNN(Adam)	0.1263	0.1153	0.9869
8	CNN(RMSprop)	0.1292	0.2975	0.9796

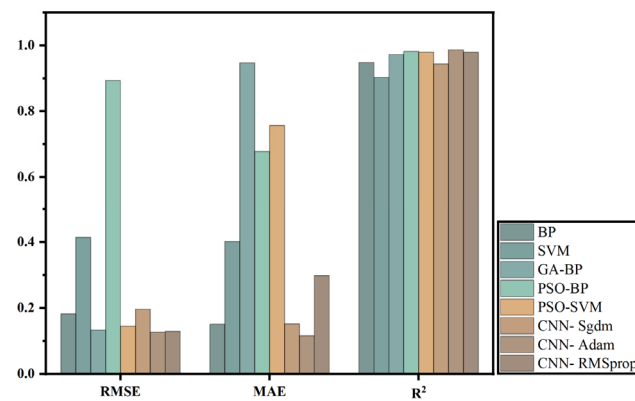


Figure 11. GWP data-driven model data schematization.

In terms of deep learning models versus traditional regression models, CNN(Adam) reduces 0.0554, 0.2878, 0.0062, 0.7671, and 0.0184 in terms of RMSE compared to BP, SVM, GA-BP, PSO-BP, and PSO-SVM, respectively. MAE decreased by 0.0348, 0.286, 0.8318, 0.5621, and 0.6415, respectively. As for R^2 , CNN(Adam) ranked the highest. The above analytical study shows that the CNN(Adam) algorithm outperformed all other data-driven models in predicting the error of the network prediction model concerning the data. It had the highest R^2 score and the smallest RMSE and MAE values. This means that CNN(Adam) can be better generalized to new sample data and can be effectively used to predict data for building GWP.

5.5. LCC Prediction Model Visualization Results

The training process of the LCC convolutional neural network model for the Turpan office building is shown in Figure 12.

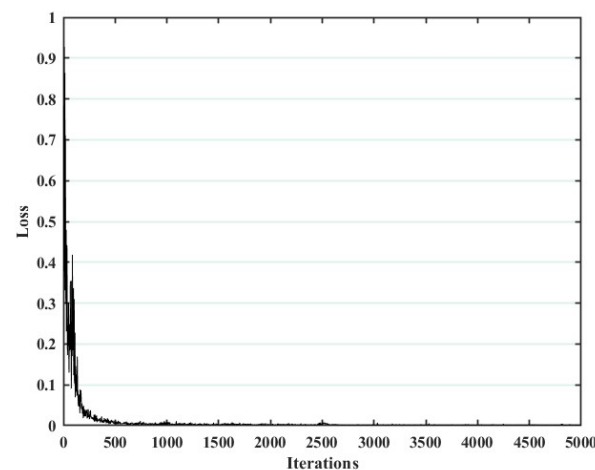
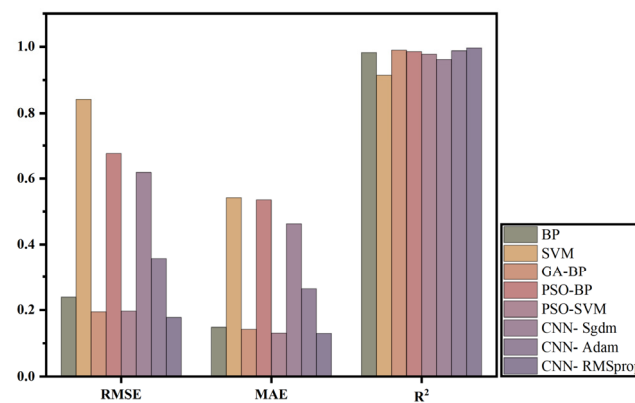


Figure 12. The CNN model training process for LCC.

Analysis: In terms of building LCC, the eight building performance models are shown in Table 8. Also, the results of R^2 , RMSE, and MAE are shown in Figure 13. It is found through the figure that, among the eight models, the CNN(RMSprop) model has the highest correlation coefficient and the lowest RMSE and MAE. At the same time, other evaluation models have shown some advantages. The building performance modeling accuracy (R^2) sizes are in order: CNN(RMSprop), GA-BP, CNN(Adam), PSO-BP, BP, PSO-SVM, CNN(Sgdm), SVM. Additionally, the order of size in terms of RMSE evaluation metrics is as follows: CNN(RMSprop), GA-BP, PSO-SVM, BP, CNN(Adam), CNN(Sgdm), PSO-BP, SVM. Finally, the order of magnitude in terms of MAE evaluation metrics is as follows: CNN(RMSprop), PSO-SVM, GA-BP, BP, CNN(Adam), CNN(Sgdm), PSO-BP, SVM.

Table 8. LCC data-driven model accuracy visualization results.

Sort	Model	RMSE	MAE	R ²
1	BP	0.2387	0.1482	0.9824
2	SVM	0.8413	0.5415	0.9145
3	GA-BP	0.1945	0.1421	0.9899
4	PSO-BP	0.6756	0.5348	0.9856
5	PSO-SVM	0.1965	0.1307	0.9775
6	CNN(Sgdm)	0.6187	0.4632	0.9616
7	CNN(Adam)	0.3572	0.2639	0.9881
8	CNN(RMSprop)	0.1772	0.1295	0.9969

**Figure 13.** LCC data-driven model accuracy visualization results.

In terms of deep learning models versus traditional regression models, CNN(RMSprop) is reduced by 0.0615, 0.6641, 0.0173, 0.4984, and 0.0193 in terms of RMSE compared to BP, SVM, GA-BP, PSO-BP, and PSO-SVM, respectively. MAE is decreased by 0.0187, 0.412, 0.0126, 0.4053, and 0.0012, respectively. As for R², CNN(RMSprop) is ranked the highest. The above analytical study shows that the CNN(RMSprop) algorithm outperforms all other data-driven models in predicting the error of the network prediction model concerning the data. It has the highest R² score and the smallest RMSE and MAE values. This means that the CNN(RMSprop) can be better generalized to new sample data and can be effectively used to predict data for building LCC.

Summary: In terms of time cost, CNN prediction models can significantly reduce time cost compared to baseline models (parametric performance models created by Rhino software). In terms of energy prediction, the CNN prediction model takes only 129 s for a single run compared to 21.57 min if a traditional arithmetic model (baseline model) is used. A comprehensive comparison reveals that CNN(Adam) reduces the time cost by 90.21%. For GWP prediction, the CNN prediction model takes only 149 s to run once, while the baseline model takes 27.45 min. A comprehensive comparison reveals that CNN(Adam) reduces the time cost by 91.06%. For LCC prediction, the CNN prediction model takes only 138 s to run once, while the baseline model takes 23.29 min. A comprehensive comparison reveals that CNN(RMSprop) reduces the time cost by 90.20%, as shown in Figure 14. It can be concluded that the efficiency of the model can be greatly improved and the time cost can be saved by the method based on deep learning model prediction.

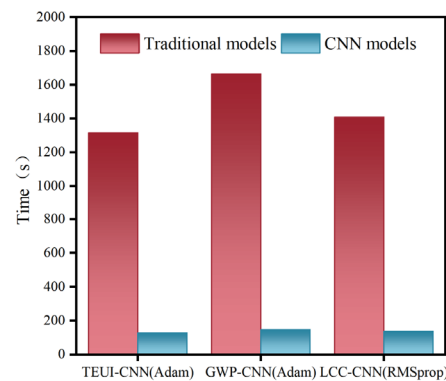


Figure 14. The plot of TEUI, GWP, and LCC data-driven models against baseline model time.

5.6. Visualization of Multi-Objective Optimization Results

5.6.1. Three Types of Objective Function Analysis

As shown in Figure 15, in this paper the NSGA-II algorithm is used for multi-objective optimization. After traversing the data for 100 generations, a sample set of 4500 is obtained. The distribution of the three target indicators (TEUI, GWP, and LCC) is shown in Figure 11. A study and analysis of the optimized solution set (independent parameter-objective variable) shows the range of distribution of the three objectives TEUI, GWP, and LCC. In terms of TEUI, the data are mainly distributed between 148.25 kWh/m² and 165.22 kWh/m². In terms of GWP, the data are mainly distributed between 67.82 kg/m² and 77.97 kg/m². In terms of LCC, the values are mainly concentrated between 178,407.20 CNY/m²–189,508.02 CNY/m². The three target values for the original office building are a TEUI of 198.89 kWh/m², a GWP of 91.51 kg/m², and an LCC of 267,731.96 CNY/m². After the optimization of the objectives, the optimal index and the original building index are reduced by 108.53 kWh/m², 47.31 kg/m², and 84,537.83 CNY/m², respectively. The three target values were reduced by 41.94%, 40.61%, and 31.29%, respectively.

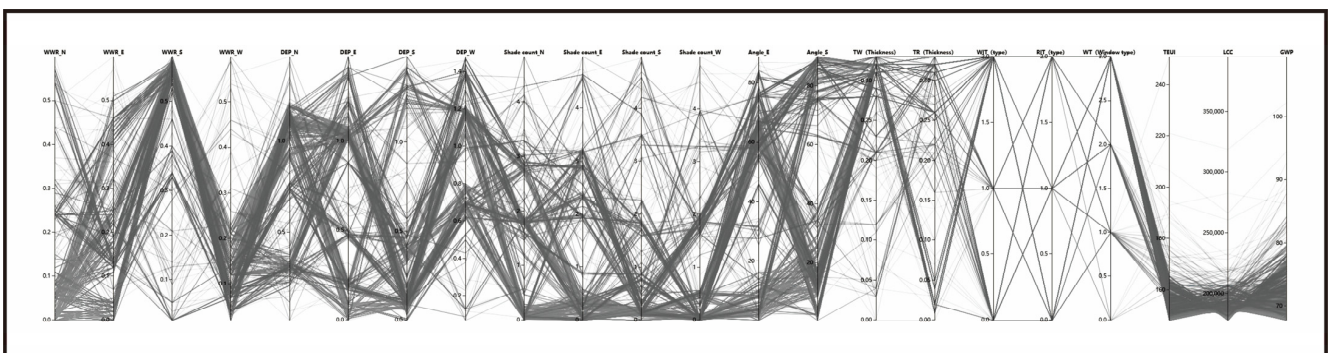


Figure 15. The plot of total data results for 4500 multi-objective optimizations.

5.6.2. Analysis of Variables

Based on the obtained 45 Pareto solutions in parallel coordinate plots, the distribution of each variable can be seen, as shown in Figure 16. In terms of insulation type, WIT is focused on EPS and PU, and RIT is focused on PU. Optimization variables show that exterior walls have a wider range of insulation options compared to roofs. This is mainly due to the large area of building coverage on the exterior walls compared to the roof. Although EPS has a poor thermal performance compared to XPS and PU. However, in the case of large office buildings with large surface areas, coupled with relatively affordable prices, EPS has a significant advantage in terms of economic cost.

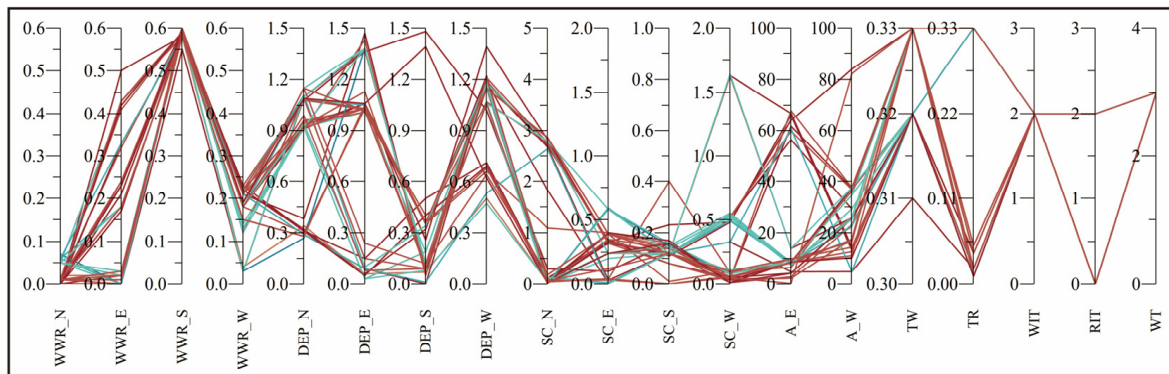


Figure 16. Distribution of variables for 45 Pareto optimization schemes.

Analysis in terms of insulation thickness. TW is mainly distributed around 0.32 and TR between 0.02 and 0.11. Analyze the reasons for its existence in a cold region like Turpan, where winters are cold and summers are hot. Since it has very strong solar radiation, take the maximum number of uses at the TW insulation level.

In terms of window types, the last option was chosen for all scenarios. The reason for this is that it has a small heat transfer coefficient, which effectively prevents heat loss in winter. It also has a relatively high SHGC, which increases the absorption of solar radiation in office buildings in winter. In addition to this, WT with good thermal performance has a profound impact on the life cycle of office buildings in cold regions like Turpan.

In terms of WWR distribution. The distributions of WWR_S and WWR_N are more concentrated compared to WWR_W and WWR_E, which are distributed around 0.55 and 0.01, respectively. This allows the building to receive more solar radiation in the winter, allowing more heat to be gained inside while avoiding heat loss. For high-latitude places like Turpan, where buildings in the region are more susceptible to western sunlight, which in turn leads to overheating indoors, WWR_W has a smaller distribution than WWR_E. Therefore reducing WWR_W minimizes the cooling energy consumption of the air conditioner in the summer and also reduces the LCC and GWP.

In terms of shade depth, DEP_S is mainly distributed between 0 and 0.3, and DEP_E is mainly distributed around 1.1; additionally, their average values are lower than those of DEP_N and DEP_W. The reason for this is that increasing the length of shading at these two levels of this office building, although it reduces the entry of hot outdoor heat into the interior during the summer months, has the negative effect of making the interior less thermally comfortable during the winter months. Meanwhile, in terms of WWR_E and WWR_W, their values are relatively widely distributed due to the long summer period in Xinjiang. West-facing shading can effectively improve indoor thermal comfort while also reducing energy consumption and economic costs.

5.7. Analysis of Entropy-Based Evaluation Models for the Topsis Method

In evaluating the 45 programs on the Pareto frontier using the entropy-based Topsis method, the target metrics are first selected. That is, TEUI, GWP, and LCC are selected in this paper. Secondly, the type of indicator is established, and the three indicators selected in this paper are all of the very small value type. That is, the smaller the value representing the Turpan office building performance capacity, the better, and the more environmentally friendly the energy-saving emission reduction adjustment ability will be. In the third step, information on the various indicators for the three objectives is established, as shown in Table 9 below.

Table 9. Indicator information for the three objectives of the entropy weighting method.

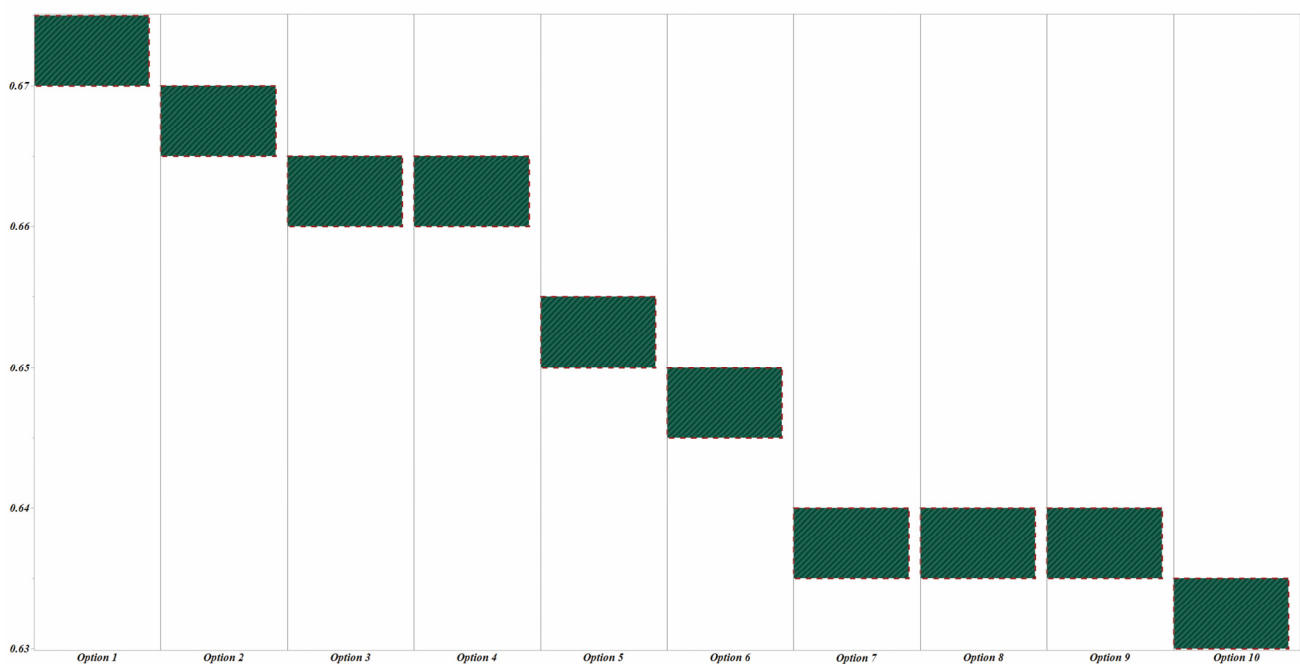
Type	Total Energy Consumption (TEUI)	Global Warming Potential (GWP)	Life Cycle Costs (LCC)
Information entropy values (e)	0.955	0.954	0.962
Information utility value (d)	0.045	0.046	0.038
Weights (%)	35.10	35.63	29.27

Table 10 shows the matrix calculation information for the Topsis method. The ranking data information for each target scenario was analyzed and compiled based on the Topsis methodology. Meanwhile, Table 10 shows the top 10 highest-rated results.

Table 10. Entropy-based Topsis method program data information (Top 10).

Optimal Type	Positive Ideal Solution (D+)	Negative Ideal Solution (D−)	Composite Score	Sort
Option 1	0.368924	0.758328	0.672722	1
Option 2	0.387277	0.780325	0.668314	2
Option 3	0.352599	0.695340	0.663531	3
Option 4	0.389703	0.760765	0.661266	4
Option 5	0.375661	0.712357	0.654729	5
Option 6	0.375361	0.685431	0.646150	6
Option 7	0.474827	0.839538	0.638740	7
Option 8	0.371605	0.656131	0.638423	8
Option 9	0.371808	0.649367	0.635901	9
Option 10	0.450525	0.782468	0.634609	10

Analysis: Visualize the above table in a graph. As shown in Figure 17, the higher the square block rises, the higher the score for the program. As can be seen from the graph, option 1 scored 0.672722, which is the highest score. It has an optimal solution: TEUI is 150.23 kWh/m², GWP is 69.20 kg/m² and LCC is 185,654.18 CNY/m².

**Figure 17.** Graphical representation of data information for each scenario of the entropy-based Topsis method.

5.8. Evaluation Model Analysis of the Topsis Method Based on Subjective Empowerment

The program ranking scores are analyzed in this subsection by varying the weighting factors. Based on changing different weighting factors, two schemes are derived from this: The first one is to set TEUI, GWP, and LCC as preferred targets in order, with preferred targets weighted at 1 and others at 0. The second option is to assign 0.33 to each of the three indicators to visualize the study analysis.

5.8.1. The First Empowerment Scheme

Analysis: In terms of TEUI, it is shown in Table 11. The optimal solution score is 1. The corresponding optimal solutions are WIT for PU, RIT for EPS, WT for Triple pane Low-e(green), WWR_N for 0.05, WWR_E for 0.01, WWR_S for 0.59, WWR_W for 0.03, DEP_N for 1.11 m, DEP_E for 1.38 m, DEP_S for 0.12 m, DEP_W for 1.06 m, SC_N for 0, SC_E for 0, SC_S for 0, SC_W for 1, A_E for 8.52°, A_W for 25.76°, TW for 0.33 m, TR for 0.02 m, TEUI for 148.25 kWh/m², GWP for 67.92 kg/m², and LCC for 188,149.84 CNY/m².

Table 11. Graphical representation of the top 10 program rankings when TEUI weight information is 1.

Optimal Type	Positive Ideal Solution (D+)	Negative Ideal Solution (D−)	Composite Score	Sort
Option 1	0.000000	0.999988	1.000000	1
Option 2	0.003536	0.996452	0.996464	2
Option 3	0.011905	0.988084	0.988095	3
Option 4	0.039309	0.960679	0.960691	4
Option 5	0.043257	0.956731	0.956742	5
Option 6	0.067008	0.932981	0.932992	6
Option 7	0.074139	0.925850	0.925860	7
Option 8	0.082979	0.917009	0.917020	8
Option 9	0.110913	0.889075	0.889085	9
Option 10	0.116925	0.883064	0.883074	10

In terms of GWP, as shown in Table 12, the optimal solution score is 1. The corresponding optimal solutions are WIT for PU, RIT for PU, WT for Triple pane Low-e(green), WWR_N for 0.01, WWR_E for 0.01, WWR_S for 0.55, WWR_W for 0.03, DEP_N for 1.11 m, DEP_E for 1.37 m, DEP_S for 0.12 m, DEP_W for 1.19 m, SC_N for 2, SC_E for 0, SC_S for 0, SC_W for 2, A_E for 13.97°, A_W for 25.66°, TW for 0.32 m, TR for 0.02 m, TEUI for 148.31 kWh/m², GWP for 67.82 kg/m², and LCC for 189,508.02 CNY/m².

Table 12. Graphical representation of the top 10 program rankings when GWP weight information is 1.

Optimal Type	Positive Ideal Solution (D+)	Negative Ideal Solution (D−)	Composite Score	Sort
Option 1	0.000000	0.999980	1.000000	1
Option 2	0.004948	0.995032	0.995052	2
Option 3	0.009693	0.990287	0.990307	3
Option 4	0.052566	0.947414	0.947432	4
Option 5	0.072996	0.926984	0.927002	5
Option 6	0.078864	0.921117	0.921135	6
Option 7	0.101570	0.898411	0.898428	7
Option 8	0.122356	0.877624	0.877642	8
Option 9	0.135865	0.864116	0.864133	9
Option 10	0.172855	0.827125	0.827142	10

In terms of LCC, as shown in Table 13. The optimal solution score is 1. The corresponding optimal solutions are WIT for PU, RIT for EPS, WT for Triple pane Low-e(green),

WWR_N for 0.01, WWR_E for 0.50, WWR_S for 0.58, WWR_W for 0.21, DEP_N for 0.38 m, DEP_E for 1.47 m, and DEP_S for 0.07 m, DEP_W is 1.19 m, SC_N is 3, SC_E is 0, SC_S is 0, SC_W is 0, A_E is 64.12°, A_W is 83.90°, TW is 0.33 m, TR is 0.02 m, TEUI is 165.22 kWh/m², GWP is 77.97 kg/m², and LCC is 178,407.20 CNY/m².

Table 13. Graphical representation of the top 10 program rankings when the LCC weight information is 1.

Optimal Type	Positive Ideal Solution (D+)	Negative Ideal Solution (D−)	Composite Score	Sort
Option 1	0.000000	1.000000	1.000000	1
Option 2	0.003347	0.996653	0.996653	2
Option 3	0.018799	0.981201	0.981201	3
Option 4	0.043928	0.956072	0.956072	4
Option 5	0.063234	0.936766	0.936766	5
Option 6	0.081126	0.918874	0.918874	6
Option 7	0.119132	0.880868	0.880868	7
Option 8	0.124258	0.875742	0.875742	8
Option 9	0.149042	0.850958	0.850958	9
Option 10	0.154563	0.845437	0.845437	10

5.8.2. The Second Empowerment Scheme

In this subsection, TEUI, GWP, and LCC are visualized and analyzed with weights set to 0.33, as shown in Table 14.

Table 14. Graphical representation of data information for three targets with weight information of 0.33 (Top 10).

Optimal Type	Positive Ideal Solution (D+)	Negative Ideal Solution (D−)	Composite Score	Sort
Option 1	0.390863	0.740950	0.654658	1
Option 2	0.366709	0.683724	0.650897	2
Option 3	0.411852	0.760994	0.648844	3
Option 4	0.413608	0.742166	0.642138	4
Option 5	0.394783	0.697264	0.638493	5
Option 6	0.391516	0.672434	0.632017	6
Option 7	0.382523	0.646877	0.628402	7
Option 8	0.381307	0.641183	0.627080	8
Option 9	0.506743	0.815601	0.616784	9
Option 10	0.479964	0.760820	0.613177	10

As shown in Table 14, the optimal solution score is 0.654658 under this scheme. The corresponding optimal solutions are WIT for PU, RIT for EPS, WT for Triple pane Low-e(green), WWR_N for 0.05, WWR_E for 0.02, WWR_S for 0.59, WWR_W for 0.14, DEP_N for 0.92 m, DEP_E for 0.03 m, DEP_S for 0.19 m, DEP_W is 1.18 m, SC_N is 0, SC_E is 0, SC_S is 0, SC_W is 1, A_E is 8.52°, A_W is 34.65°, TW is 0.33 m, TR is 0.01 m, TEUI is 150.23 kWh/m², GWP is 69.20 kg/m², and LCC is 185,654.18 CNY/m².

5.9. Comparative Analysis between Optimal Solutions

The three objectives of the Pareto frontier solution are sequentially ranked, using the entropy-based Topsis method and subjective assignment. Obtain five solutions to visualization: Topsis optimal, TEUI optimal, GWP optimal, LCC optimal, and each of the three objective value weights is 0.33, as shown in Table 15.

Table 15. Optimal Solution Objective Indicators and Distribution of Variables.

Categories	TOPSIS Optimal	TEUI Optimal	GWP Optimal	LCC Optimal	Weighting 0.33 Each
WIT	PU	PU	PU	PU	PU
RIT	EPS	EPS	PU	EPS	EPS
WT	Triple pane Low-e(green)				
WWR_N	0.05	0.05	0.01	0.01	0.05
WWR_E	0.02	0.01	0.01	0.50	0.02
WWR_S	0.59	0.59	0.55	0.58	0.59
WWR_W	0.14	0.03	0.03	0.21	0.14
DEP_N	0.92	1.11	1.11	0.38	0.92
DEP_E	0.03	1.38	1.37	1.47	0.03
DEP_S	0.19	0.12	0.12	0.07	0.19
DEP_W	1.18	1.06	1.19	1.19	1.18
SC_N	0	0	2	3	0
SC_E	0	0	0	0	0
SC_S	0	0	0	0	0
SC_W	1	1	2	0	1
A_E	8.52	8.52	13.97	64.12	8.52
A_W	34.65	25.76	25.66	83.90	34.65
TW	0.33 m	0.33 m	0.32 m	0.33 m	0.33 m
TR	0.01 m	0.02 m	0.02 m	0.02 m	0.01 m
TEUI	150.23	148.25	148.31	165.22	150.23
GWP	69.20	67.92	67.82	77.97	69.20
LCC	185,654.18	188,149.84	189,508.02	178,407.20	185,654.18

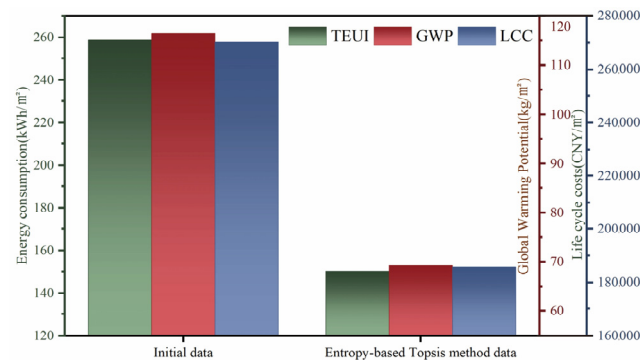
As can be seen from the above table, for the entropy-based Topsis method, the TEUI is 150.23 kWh/m², the GWP is 69.20 kg/m², and the LCC is 185,654.18 CNY/m². In terms of optimal TEUI, the TEUI is 148.25 kWh/m², GWP is 67.92 kg/m², and LCC is 188,149.84 CNY/m². In terms of optimal GWP, the TEUI is 148.31 kWh/m², GWP is 67.82 kg/m², and LCC is 189,508.02 CNY/m². In terms of LCC optimization, TEUI is 165.22 kWh/m², GWP is 77.97 kg/m², and LCC is 178,407.20 CNY/m². For each of the three target value weights of 0.33 scenarios, TEUI is 150.23 kWh/m², GWP is 69.20 kg/m², and LCC is 185,654.18 CNY/m².

6. Article Discussion

6.1. Comparative Analysis of Data with the Original Office Building Program

6.1.1. Comparison of the Results of the Optimal Scheme of the Entropy-Based Topsis Method with the Initial Data

From Section 4.5.1, the TEUI of the original office building is 258.76 kWh/m², the GWP is 116.51 kg/m², and the LCC is 270,192.01 CNY/m². After comparing the optimal solution with the entropy-based Topsis method, it is shown in Figure 18. The TEUI of the office building was reduced by 108.53 kWh/m², the GWP by 47.31 kg/m², and the LCC by 84,537.83 CNY/m². The TEUI, GWP, and LCC were reduced by 41.94%, 40.61%, and 31.29%, respectively.

**Figure 18.** Comparison of the optimal entropy-based Topsis method with initial building data.

6.1.2. Comparison of the Results of the Optimal TEUI-Based Scheme with the Initial Data

In the optimal TEUI scheme, as shown in Figure 19, the optimal TEUI for office buildings is 148.25 kWh/m². Compared with the original building TEUI, the reduction is 110.51 kWh/m², which is 42.71% energy saving.

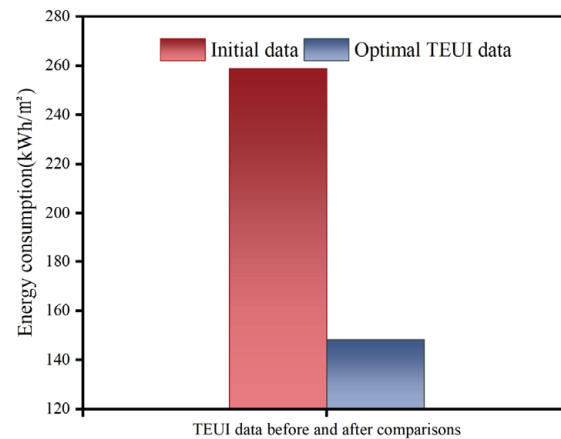


Figure 19. Comparison of TEUI optimal solution with initial building data.

6.1.3. Comparison of the Results of the Optimal GWP-Based Scheme with the Initial Data

In the optimal GWP scheme, this GWP consists of two parts, i.e., the carbon dioxide emissions during the initial phase cycle (CO₂_DLC) and the carbon dioxide emissions during the operational phase cycle (CO₂_OP) of this Turpan office building. As shown in Figure 20, the optimal GWP value of the office building is 69.20 kg/m², CO₂_DLC is 143,209.39 kgCO₂, and CO₂_OP is 3,247,800 kgCO₂, while the GWP of the original building is 116.51 kg/m², CO₂_DLC is 294,752 kgCO₂, and CO₂_OP is 5,530,748 kgCO₂. The comparison shows that GWP is reduced by 47.31 kg/m², CO₂_DLC is reduced by 151,542.60 kgCO₂, and CO₂_OP is reduced by 2,282,948 kgCO₂. They were reduced by 40.61%, 51.41%, and 41.28%, respectively.

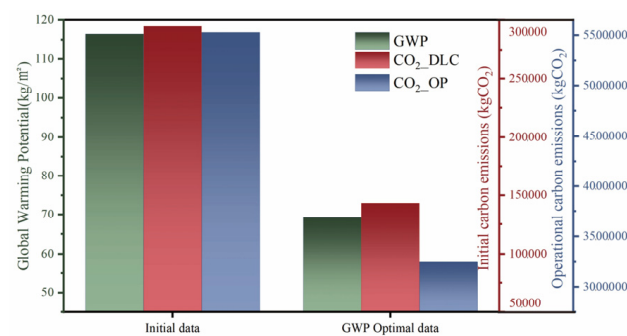


Figure 20. Comparison of GWP optimal solution with initial building data.

6.1.4. Comparison of the Results of the Optimal LCC-Based Scheme with the Initial Data

In the optimal LCC scheme, as shown in Figure 21. The LCC of this scheme is 178,407.20 CNY/m² and the building operating cost (EC) is 240,006 CNY. Compared to the original LCC, the LCC was reduced by 91,784.81 CNY/m² and the EC was reduced by 122,473 CNY. They were reduced by 33.97% and 33.79%, respectively.

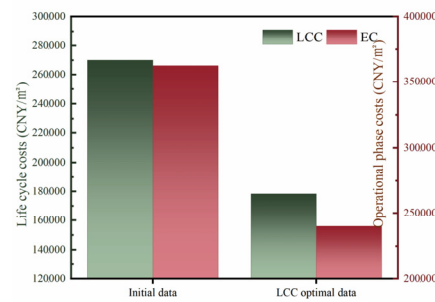


Figure 21. Comparison of LCC optimal solution with initial building data.

6.2. Visualization of Sensitivity Analysis

The Pareto frontier solution can only give the set of regional solutions within the optimal range of the three metrics, but it does not give information about the ranked situation or the importance of the characteristics of the parameters of the independent variables. Therefore, on this basis, this paper uses the sensitivity analysis strategy to define the degree of influence of the parameters of the independent variables on the target variables. After the methodology has been used to derive the degree of influence between the variables, it can be used as a basis for further screening under specific conditions and the prioritization of important parameters, which enhances the performance of the office building. At the level of sensitivity analysis carried out in this article, the article uses two different schemes, the RBD-FAST and DMIM methods.

6.2.1. RBD-FAST Methodology Analysis

In the RBD-FAST method, for the variables affecting TEUI, the top four are TR > WWR_W > WWR_E > TW. These four variables account for 43.31% of the overall, as shown in Figure 22a. For GWP, the top four influences are TR > WWR_W > WWR_E > TW. These four variables accounted for 85.96% of the total, as shown in Figure 22b. In terms of LCC, the top four influences are TR > TW > WT > SC_E, respectively. These four variables accounted for 88.75% of the total, as shown in Figure 22c.

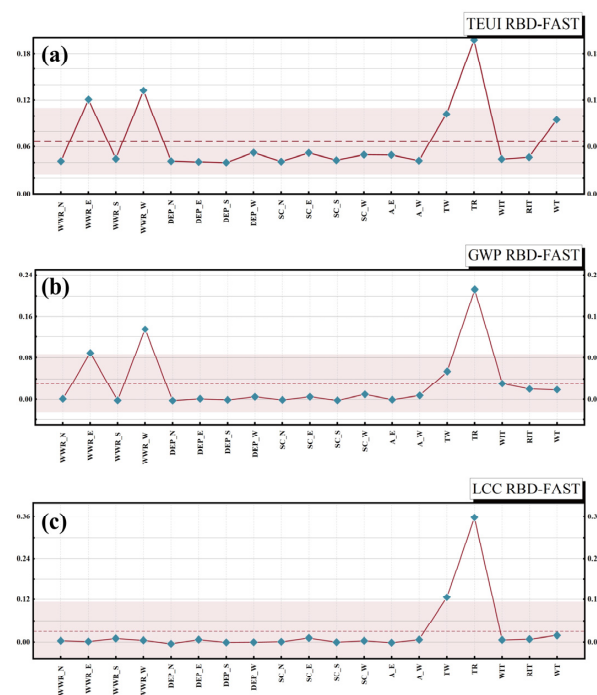


Figure 22. RBD-FAST method analysis. (a) TEUI results visualization. (b) GWP results visualization. (c) LCC results visualization.

6.2.2. DMIM Methodology Analysis

In the DMIM sensitivity approach, as shown in Figure 23, for TEUI, the top four TOI and FOI rankings are TR > WWR_W > WWR_E > TW and TR > TW > WWR_W > WWR_E, respectively. They represent 43.30% and 80.30% of the TOI and FOI as a whole, respectively.

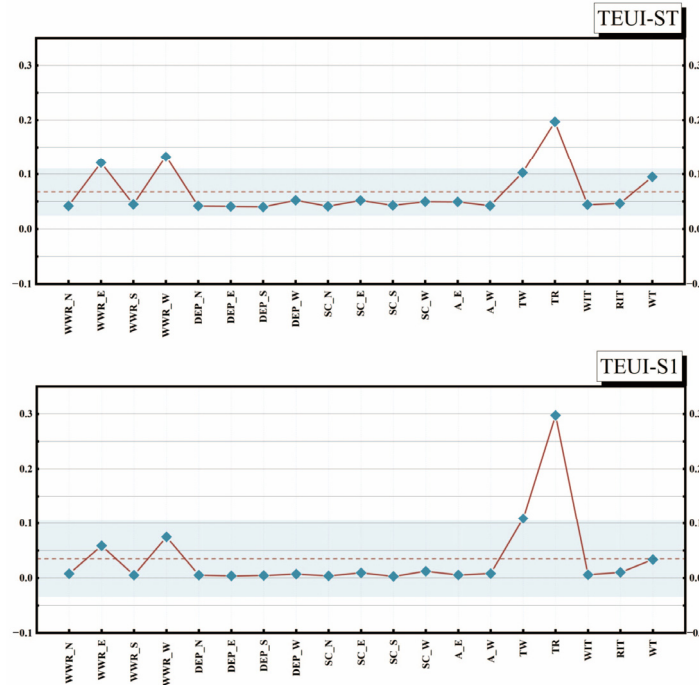


Figure 23. Visualization of the DMIM method analysis of TEUI.

For GWP, the top four TOI and FOI rankings are WWR_W > WWR_E > TR > WIT and TR > WWR_W > WWR_E > TW, respectively. These four variables accounted for 41.12% and 73.13% of the overall TOI and FOI, respectively. Figure 24 shows the results of the analytical visualization of the DMIM method for GWP.

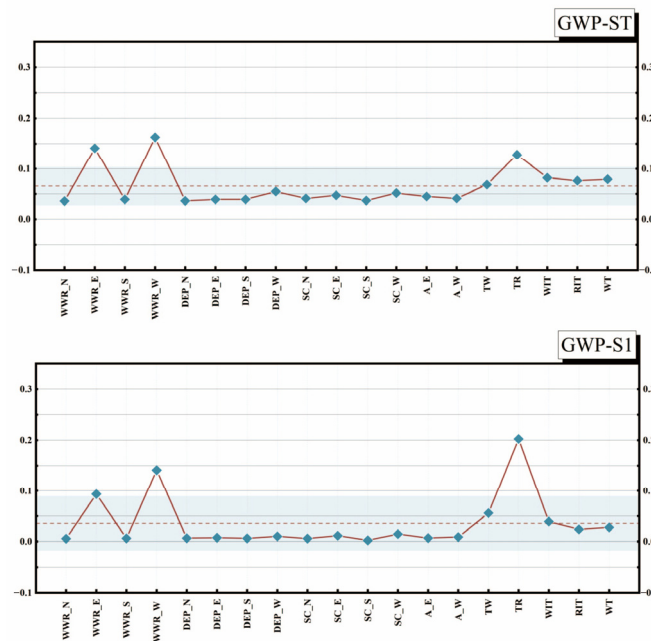


Figure 24. Visualization of the DMIM method analysis of GWP.

For LCC, the top four TOI and FOI rankings are $TR > TW > WT > WWR_W$ and $TR > TR > TW > WT > SC_E$, respectively. They accounted for 34.38% and 82.25% of the overall TOI and FOI, respectively. Figure 25 shows the results of the analytical visualization of the DMIM method for LCC.

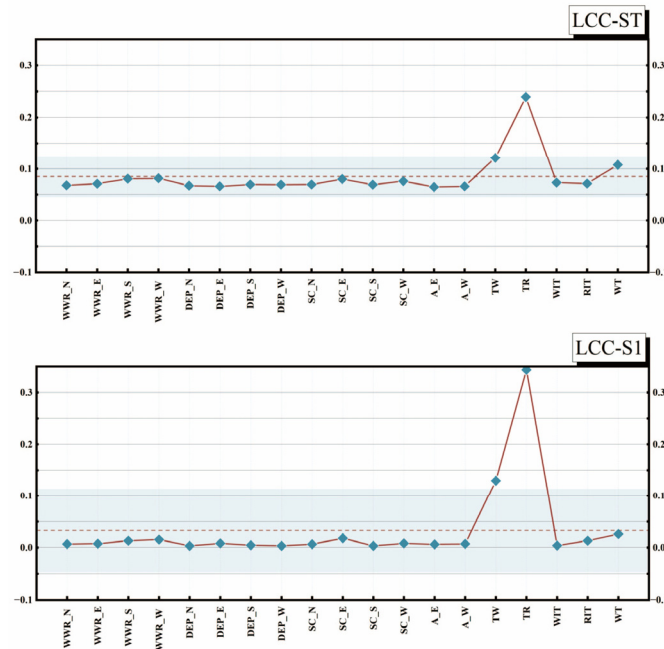


Figure 25. Visualization of the DMIM method analysis of LCC.

6.2.3. Analysis of Results

For TEUI and GWP, the big impacts are TR, WWR_W, and WWR_E. More attention should be paid to the TR aspect of the design in future building construction. The design can be carried out in such a way as to increase the TR according to the specific construction. In addition, when building a new construction or remodeling, designers should be more likely to consider the impact of WWR_W and WWR_E on the performance of office buildings. Shading not only reduces the TEUI of office buildings but also reduces carbon emissions. It is also in line with the “dual-carbon” policy that China has proposed in recent years. In terms of LCC, increasing TR with TW is an optimized form of measurement to reduce LCC. A modest increase in TR and TW will allow office buildings to reduce some of the solar radiation during the summer months. It also provides insulation in the winter months. In the long run, the impact on the performance characteristics of office buildings in the region will be far-reaching. SC_N and SC_S are ranked very close to 0 for the three target indicator impacts. Therefore, the above two independent variable parameters have little impact on the results of the study when conducting the design, and the designer can make trade-offs according to the specific scenario when making decisions.

6.3. Comparison and Linkage of Findings to Existing Research

6.3.1. At the Level of Multi-Objective Optimization

The starting point of the research content of this paper is to optimize the TEUI, GWP, and LCC of the building and analyze them using the NSGA-II algorithm, then go on to provide a guiding idea for the optimization of the building performance in extremely hot and cold regions. The results of the study show that, when optimizing the performance objectives (TEUI, GWP, and LCC), the WWR_N and WWR_S of the building are presented as minimized and maximized, respectively. This optimization can result in a building that can gain more heat in the winter while also reducing heat loss. Existing studies have found that Zhang et al. went about studying office building GWP and LCC by utilizing the NSGA-II algorithm [22]. Song et al. used the NSGA-II algorithm to optimize the LCC and HTD

(hours of thermal discomfort) for residential buildings in Turpan [98]. The multi-objective optimization results of the above two scholars are consistent with this paper. That is, the distribution of WWR_N and WWR_S is the most concentrated, and WWR_N and WWR_S show the tendency of minimization and maximization in the multi-objective optimization process. It can be seen that, especially in very hot and cold regions and severe cold regions, WWR has a great influence on the building performance when optimizing the building performance in a multi-objective way. Therefore, the impact of WWR on buildings should be considered in future designs.

6.3.2. At the Level of Decision Analysis

The article uses two decision analysis methods, the entropy-based Topsis method, and the subjective empowerment Topsis method. In this case, when the entropy-based Topsis method is used, the optimization results in a reduction in the TEUI, GWP, and LCC of 41.94%, 40.61%, and 31.29%, respectively. Literatures [37,98] used the entropy-based Topsis method to go for the effect of optimization of building energy efficiency in extremely hot and cold regions and severe cold regions, respectively. In the above optimization results, in terms of building performance improvement strategies at the level of the building envelope, at the level of the building shading measures, and at the level of the building's thermal insulation performance, the method objectively evaluates and measures the optimization results to quickly and efficiently improve the building's performance potential. Thus, they can provide some advice to the designers involved in the analysis phase of future decisions.

6.3.3. At the Level of Sensitivity Analysis

The article uses two sensitivity analyses to investigate the effect of independent variable parameters on building performance goals. It was found that, for reducing the TEUI, GWP, and LCC, the optimized measure is the selection of high-performance windows. The optimization in this paper results in the use of Triple pane, Low-e(green) type windows. Secondly, increasing the WWR_S and decreasing the WWR_N and WWR_E of a building is critical to improving building performance. Literatures [37,98] are more consistent at the level of performance sensitivity analysis compared to the results derived from the optimization in this paper. It can be seen that window performance and the WWR of a building have a very significant effect on building performance, so more attention should be paid to this aspect in future research.

6.4. Limitations of Future Research

In the framework content studied in this paper, the internal heat flow direction in office buildings is not considered. Subsequent research could look at issues related to heat flow inside buildings in terms of fluid dynamics. Also, in terms of the building's internal wind environment, a good wind environment direction can improve the indoor air quality and enhance the comfort of office workers. Therefore, it can also be included in the analysis of subsequent studies. Analyzed in terms of life cycle stages, the dismantling stage can be added to the study in subsequent research. Changes in various economic cost rates over time can also affect LCC. The unexplored life cycle years of office buildings in extremely hot and cold regions can have a direct impact on GWP and LCC. In addition, the development of passive technologies has been accompanied by subtle changes in building performance, e.g., the economic costs and carbon emissions associated with improved thermal insulation and changes in high-performance windows, which in turn lead to improvements in building airtightness, are difficult to demonstrate quantitatively at the initial investment stage and will still require some realistic assessment and measurement in future research.

7. Conclusions

7.1. Applicability of the Article's Research

In the course of the research in this paper, the content of the framework is not immutable; it is malleable. For example, this article examines the energy consumption, CO₂ emissions, and economics of office buildings in Turpan only. Subsequent studies could add other performance metrics to this, such as optical performance indicators and thermal comfort indicators (PMV, UTCI, PET, SET). Additionally, research from different climate zone levels can have more options and applications. At the same time, the content of the framework studied in this paper is variable. For example, when considering a larger number of independent variable parameters and multiple performance targets, a sensitivity analysis can be performed to retain the more influential independent variable parameters. This greatly reduces the time spent on analysis, which in turn improves the efficiency of building performance. In addition to this, other MCDM methods can be added when a larger number of performance objectives needs to be considered. Analysis through multiple methods at the decision-making stage can, in turn, increase the transparency and credibility of decisions.

7.2. Article Conclusions

This paper takes the optimization of office building performance prediction in the Turpan area as the research objective. It uses TEUI, GWP, and LCC as the target indicators for performance prediction optimization analysis, and then proceeds to explore the energy-saving strategies in performance prediction optimization of office buildings in the cold region of Turpan. The conclusions of the article are divided into the following areas:

- (1) This paper creates three deep neural network data-driven prediction models based on office building performance objectives (TEUI, GWP, and LCC). In this analysis, each performance metric was compared using eight separate data-driven models for prediction. Finally, in the prediction results, the optimal data-driven model in terms of TEUI is CNN(Adam), which is a deep learning model with R^2 of 0.9908, RMSE of 0.1871, and MAE of 0.1254. In terms of GWP, the optimal data-driven model is CNN(Adam), which is a deep learning model with an R^2 of 0.9869, RMSE of 0.1263, and MAE of 0.1153. In terms of LCC, the optimal data-driven model is CNN(RMSprop), which is a deep learning model with R^2 of 0.9969, RMSE of 0.1772, and MAE of 0.1295.
- (2) In this paper, a multi-objective optimization of the performance objectives of office buildings in the Turpan region is carried out. The article uses the NSGA-II optimization algorithm to optimize the three objectives. The optimized three objectives were then compared against the initial data for the office building. The results of the analysis were as follows: The TEUI was reduced by 108.53 kWh/m² from the initial value, and its reduction was 41.94%. The GWP was reduced by 43.71 kg/m² from the initial value, and its reduction was 40.61%. The LCC was reduced by 84,537.83 CNY/m² from the initial value and its reduction was 31.29%.
- (3) In the program decision part, this paper adopts the entropy-based Topsis method and subjective empowerment method for decision analysis. In the entropy-based Topsis method scheme, the three metrics of the optimal solution are TEUI of 150.23 kWh/m², GWP of 69.20 kg/m², and LCC of 185,654.18 CNY/m². In the subjective assignment method, the three target indicators of the optimal TEUI scheme are 148.25 kWh/m² for TEUI, 67.92 kg/m² for GWP, and 188,149.84 CNY/m² for LCC. The three target metrics for the optimal GWP scheme are TEUI of 148.31 kWh/m², GWP of 67.82 kg/m², and LCC of 189,508.02 CNY/m². The three target indicators of the optimal LCC scheme are 165.22 kWh/m² for TEUI, 77.97 kg/m² for GWP, and 178,407.20 CNY/m² for LCC. The target indicators under each of the three performance objectives weighted at 0.33 program are 150.23 kWh/m² for TEUI, 69.20 kg/m² for GWP, and 185,654.18 CNY/m² for LCC.

- (4) In the sensitivity analysis section. Two methods of analysis are used in this paper: In the RBD-FAST method, the top four variables affecting TEUI are $TR > WWR_W > WWR_E > TW$. The top four variables affecting GWP are $TR > WWR_W > WWR_E > TW$. The top four variables affecting LCC are $TR > TW > WT > SC_E$. In the DMIM method, the top four variables affecting the TEUI are $TR > WWR_W > WWR_E > TW$. The top four variables affecting GWP are $WWR_W > WWR_E > TR > WIT$. The top four variables affecting LCC are $TR > TW > WT > WWR_W$.

The above findings were analyzed mainly with office buildings in extremely hot and cold regions. In future research, the building's internal thermal comfort conditions, wind environment design, and acoustic environment design can be included in the study, which will improve the completeness and comprehensiveness of office building performance research. At the same time, the theme of this paper can be extended outwards. For example, the office building performance indicators (TEUI, GWP, and LCC) studied in this paper can be applied to time series forecasting in the future [99–103]. Finally, the research in this paper can provide references and ideas for the design of building performance in other different climate zones, such as hot summer and cold winter regions, hot summer and warm winter regions, and mild regions [104–108].

Author Contributions: Conceptualization, Y.L.; methodology, Y.L.; software, Y.L. and Y.H.; validation, Y.L. and W.W.; resources, W.W.; data curation, Y.L.; writing—original draft preparation, Y.L.; writing—review and editing, Y.L.; visualization, Y.L. and Y.H. All authors have read and agreed to the published version of the manuscript.

Funding: This research received no external funding.

Institutional Review Board Statement: Not applicable.

Informed Consent Statement: Not applicable.

Data Availability Statement: The data presented in this study are available on request from the corresponding author.

Conflicts of Interest: The authors declare no conflicts of interest.

References

- Liu, Y.; Wang, W.; Huang, Y.; Song, J.; Zhou, Z. Energy Performance Analysis and Study of an Office Building in an Extremely Hot and Cold Region. *Sustainability* **2024**, *16*, 572. [\[CrossRef\]](#)
- Valladares-Rendón, L.G.; Lo, S.-L. Passive Shading Strategies to Reduce Outdoor Insolation and Indoor Cooling Loads by Using Overhang Devices on a Building. *Build. Simul.* **2014**, *7*, 671–681. [\[CrossRef\]](#)
- Li, Z.; Peng, S.; Cai, W.; Cao, S.; Wang, X.; Li, R.; Ma, X. Impacts of Building Microenvironment on Energy Consumption in Office Buildings: Empirical Evidence from the Government Office Buildings in Guangdong Province, China. *Buildings* **2023**, *13*, 481. [\[CrossRef\]](#)
- Khahir, S.; Vakilinezhad, R. Energy and Thermal Analysis of DSF in the Retrofit Design of Office Buildings in Hot Climates. *Archit. Eng. Des. Manag.* **2022**, *19*, 642–664. [\[CrossRef\]](#)
- Heidarzadeh, S.; Mahdavejad, M.; Habib, F. External Shading and Its Effect on the Energy Efficiency of Tehran's Office Buildings. *Environ. Prog. Sustain. Energy* **2023**, *42*, e14185. [\[CrossRef\]](#)
- Al-Tamimi, N. Building Envelope Retrofitting Strategies for Energy-Efficient Office Buildings in Saudi Arabia. *Buildings* **2022**, *12*, 1900. [\[CrossRef\]](#)
- Koç, S.G.; Maçka Kalfa, S. The Effects of Shading Devices on Office Building Energy Performance in Mediterranean Climate Regions. *J. Build. Eng.* **2021**, *44*, 102653. [\[CrossRef\]](#)
- Huo, H.; Xu, W.; Li, A.; Lv, Y.; Liu, C. Analysis and Optimization of External Venetian Blind Shading for Nearly Zero-Energy Buildings in Different Climate Regions of China. *Sol. Energy* **2021**, *223*, 54–71. [\[CrossRef\]](#)
- Sun, N.; Cui, Y.; Jiang, Y.; Li, S. Lighting and Ventilation-Based Building Sun-Shading Design and Simulation Case in Cold Regions. *Energy Procedia* **2018**, *152*, 462–469. [\[CrossRef\]](#)
- Hashemi, A. Daylighting and Solar Shading Performances of an Innovative Automated Reflective Louvre System. *Energy Build.* **2014**, *82*, 607–620. [\[CrossRef\]](#)
- Hammad, F.; Abu-Hijleh, B. The Energy Savings Potential of Using Dynamic External Louvers in an Office Building. *Energy Build.* **2010**, *42*, 1888–1895. [\[CrossRef\]](#)
- Casini, M. Active Dynamic Windows for Buildings: A Review. *Renew. Energy* **2018**, *119*, 923–934. [\[CrossRef\]](#)

13. Favoino, F.; Fiorito, F.; Cannavale, A.; Ranzi, G.; Overend, M. Optimal Control and Performance of Photovoltachromic Switchable Glazing for Building Integration in Temperate Climates. *Appl. Energy* **2016**, *178*, 943–961. [[CrossRef](#)]
14. Dussault, J.-M.; Sourbron, M.; Gosselin, L. Reduced Energy Consumption and Enhanced Comfort with Smart Windows: Comparison between Quasi-Optimal, Predictive and Rule-Based Control Strategies. *Energy Build.* **2016**, *127*, 680–691. [[CrossRef](#)]
15. Cuce, E. Toward Multi-Functional PV Glazing Technologies in Low/Zero Carbon Buildings: Heat Insulation Solar Glass—Latest Developments and Future Prospects. *Renew. Sustain. Energy Rev.* **2016**, *60*, 1286–1301. [[CrossRef](#)]
16. Ihara, T.; Gustavsen, A.; Jelle, B.P. Effect of Facade Components on Energy Efficiency in Office Buildings. *Appl. Energy* **2015**, *158*, 422–432. [[CrossRef](#)]
17. Planas, C.; Cuerva, E.; Alavedra, P. Effects of the Type of Facade on the Energy Performance of Office Buildings Representative of the City of Barcelona. *Ain Shams Eng. J.* **2018**, *9*, 3325–3334. [[CrossRef](#)]
18. Zhang, H.; Cai, J.; Braun, J.E. A Whole Building Life-Cycle Assessment Methodology and Its Application for Carbon Footprint Analysis of U.S. Commercial Buildings. *J. Build. Perform. Simul.* **2023**, *16*, 38–56. [[CrossRef](#)]
19. Kim, H.; Lim, H.; Kim, J.; Roh, S. Propriety Assessment Model for Life Cycle Operational Global Warming Potential of Apartment Buildings in Korea Using Energy Efficiency and Energy Effective Area Data. *Sci. Rep.* **2023**, *13*, 2420. [[CrossRef](#)]
20. Kim, H.; Kim, J.; Roh, S. The Embodied Life Cycle Global Warming Potential of Off-Site Prefabricated Concrete Products: Precast Concrete and Concrete Pile Production in Korea. *Buildings* **2023**, *13*, 2590. [[CrossRef](#)]
21. Kim, H.; Jang, H.; Tae, S.; Kim, J. Program for Propriety Analysis of Global Warming Potential Caused by the Operational Energy Consumption of Buildings in Korea. *Indoor Built Environ.* **2023**, *32*, 815–824. [[CrossRef](#)]
22. Zhang, Z.; Wang, W.; Song, J.; Wang, Z.; Wang, W. Multi-Objective Optimization of Ultra-Low Energy Consumption Buildings in Severely Cold Regions Considering Life Cycle Performance. *Sustainability* **2022**, *14*, 16440. [[CrossRef](#)]
23. Yu, H.; Yang, W.; Li, Q.; Li, J. Optimizing Buildings' Life Cycle Performance While Allowing Diversity in the Early Design Stage. *Sustainability* **2022**, *14*, 8316. [[CrossRef](#)]
24. Wang, X.; Purohit, P. Transitioning to Low-GWP Alternatives with Enhanced Energy Efficiency in Cooling Non-Residential Buildings of China. *Mitig. Adapt. Strateg. Glob. Chang.* **2022**, *27*, 45. [[CrossRef](#)]
25. Norouzi, M.; Colclough, S.; Jiménez, L.; Gavalda, J.; Boer, D. Low-Energy Buildings in Combination with Grid Decarbonization, Life Cycle Assessment of Passive House Buildings in Northern Ireland. *Energy Build.* **2022**, *261*, 111936. [[CrossRef](#)]
26. Honarvar, S.M.H.; Golabchi, M.; Ledari, M.B. Building Circularity as a Measure of Sustainability in the Old and Modern Architecture: A Case Study of Architecture Development in the Hot and Dry Climate. *Energy Build.* **2022**, *275*, 112469. [[CrossRef](#)]
27. Zhang, H.; Hewage, K.; Prabatha, T.; Sadiq, R. Life Cycle Thinking-Based Energy Retrofits Evaluation Framework for Canadian Residences: A Pareto Optimization Approach. *Build. Environ.* **2021**, *204*, 108115. [[CrossRef](#)]
28. Akyüz, M.K.; Kafalı, H.; Altuntaş, Ö. An Analysis on Energy Performance Indicator and GWP at Airports; a Case Study. *Energy Sources Part A Recovery Util. Environ. Eff.* **2021**, *43*, 2402–2418. [[CrossRef](#)]
29. Wang, R.; Lu, S.; Feng, W.; Zhai, X.; Li, X. Sustainable Framework for Buildings in Cold Regions of China Considering Life Cycle Cost and Environmental Impact as Well as Thermal Comfort. *Energy Rep.* **2020**, *6*, 3036–3050. [[CrossRef](#)]
30. Ansah, M.K.; Chen, X.; Yang, H.; Lu, L.; Lam, P.T.I. An Integrated Life Cycle Assessment of Different Façade Systems for a Typical Residential Building in Ghana. *Sustain. Cities Soc.* **2020**, *53*, 101974. [[CrossRef](#)]
31. Longo, S.; Montana, F.; Riva Sanseverino, E. A Review on Optimization and Cost-Optimal Methodologies in Low-Energy Buildings Design and Environmental Considerations. *Sustain. Cities Soc.* **2019**, *45*, 87–104. [[CrossRef](#)]
32. Javid, A.S.; Aramoun, F.; Bararzadeh, M.; Avami, A. Multi Objective Planning for Sustainable Retrofit of Educational Buildings. *J. Build. Eng.* **2019**, *24*, 100759. [[CrossRef](#)]
33. Duprez, S.; Fouquet, M.; Herreros, Q.; Jusselme, T. Improving Life Cycle-Based Exploration Methods by Coupling Sensitivity Analysis and Metamodels. *Sustain. Cities Soc.* **2019**, *44*, 70–84. [[CrossRef](#)]
34. Hossain, M.U.; Poon, C.S. Global Warming Potential and Energy Consumption of Temporary Works in Building Construction: A Case Study in Hong Kong. *Build. Environ.* **2018**, *142*, 171–179. [[CrossRef](#)]
35. Van Ooteghem, K.; Xu, L. The Life-Cycle Assessment of a Single-Storey Retail Building in Canada. *Build. Environ.* **2012**, *49*, 212–226. [[CrossRef](#)]
36. Lei, Y.; Dong, L. Building Sustainability Assessment Model Based on Life Cycle Cost Analysis and BIM Technology. *Int. J. Environ. Sci. Technol.* **2024**, *21*, 4089–4100. [[CrossRef](#)]
37. Kazem, M.; Ezzeldin, S.; Tolba, O. Life-Cycle Cost Analysis for Façade Retrofit Measures of Residential Buildings in Cairo. *Indoor Built Environ.* **2022**, *31*, 913–928. [[CrossRef](#)]
38. Calama-González, C.M.; Symonds, P.; León-Rodríguez, Á.L.; Suárez, R. Optimal Retrofit Solutions Considering Thermal Comfort and Intervention Costs for the Mediterranean Social Housing Stock. *Energy Build.* **2022**, *259*, 111915. [[CrossRef](#)]
39. Weerasinghe, A.S.; Ramachandra, T.; Rotimi, J.O.B. Comparative Life-Cycle Cost (LCC) Study of Green and Traditional Industrial Buildings in Sri Lanka. *Energy Build.* **2021**, *234*, 110732. [[CrossRef](#)]
40. Salmerón Lissen, J.M.; Jareño Escudero, C.I.; Sánchez de la Flor, F.J.; Escudero, M.N.; Karlessi, T.; Assimakopoulos, M.-N. Optimal Renovation Strategies through Life-Cycle Analysis in a Pilot Building Located in a Mild Mediterranean Climate. *Appl. Sci.* **2021**, *11*, 1423. [[CrossRef](#)]
41. Hromada, E.; Vitasek, S.; Holcman, J.; Schneiderova Heralova, R.; Krulicky, T. Residential Construction with a Focus on Evaluation of the Life Cycle of Buildings. *Buildings* **2021**, *11*, 524. [[CrossRef](#)]

42. Belany, P.; Hrabovsky, P.; Kolkova, Z. Combination of Lighting Retrofit and Life Cycle Cost Analysis for Energy Efficiency Improvement in Buildings. *Energy Rep.* **2021**, *7*, 2470–2483. [[CrossRef](#)]
43. Yuan, Z.; Zhou, J.; Qiao, Y.; Zhang, Y.; Liu, D.; Zhu, H. BIM-VE-Based Optimization of Green Building Envelope from the Perspective of Both Energy Saving and Life Cycle Cost. *Sustainability* **2020**, *12*, 7862. [[CrossRef](#)]
44. Amini Toosi, H.; Lavagna, M.; Leonforte, F.; Del Pero, C.; Aste, N. Life Cycle Sustainability Assessment in Building Energy Retrofitting; A Review. *Sustain. Cities Soc.* **2020**, *60*, 102248. [[CrossRef](#)]
45. Xue, Z.; Liu, H.; Zhang, Q.; Wang, J.; Fan, J.; Zhou, X. The Impact Assessment of Campus Buildings Based on a Life Cycle Assessment–Life Cycle Cost Integrated Model. *Sustainability* **2019**, *12*, 294. [[CrossRef](#)]
46. Fregonara, E.; Ferrando, D.G.; Pattono, S. Economic–Environmental Sustainability in Building Projects: Introducing Risk and Uncertainty in LCCE and LCCA. *Sustainability* **2018**, *10*, 1901. [[CrossRef](#)]
47. Dwaikat, L.N.; Ali, K.N. Green Buildings Life Cycle Cost Analysis and Life Cycle Budget Development: Practical Applications. *J. Build. Eng.* **2018**, *18*, 303–311. [[CrossRef](#)]
48. Stephan, A.; Stephan, L. Life Cycle Energy and Cost Analysis of Embodied, Operational and User-Transport Energy Reduction Measures for Residential Buildings. *Appl. Energy* **2016**, *161*, 445–464. [[CrossRef](#)]
49. Schwartz, Y.; Raslan, R.; Mumovic, D. Implementing Multi Objective Genetic Algorithm for Life Cycle Carbon Footprint and Life Cycle Cost Minimisation: A Building Refurbishment Case Study. *Energy* **2016**, *97*, 58–68. [[CrossRef](#)]
50. Invidiata, A.; Ghisi, E. Life-Cycle Energy and Cost Analyses of Window Shading Used to Improve the Thermal Performance of Houses. *J. Clean. Prod.* **2016**, *133*, 1371–1383. [[CrossRef](#)]
51. Abdallah, M.; El-Rayes, K.; Liu, L. Optimizing the Selection of Sustainability Measures to Minimize Life-Cycle Cost of Existing Buildings. *Can. J. Civ. Eng.* **2016**, *43*, 151–163. [[CrossRef](#)]
52. Han, G.; Srebric, J. Comparison of Survey and Numerical Sensitivity Analysis Results to Assess the Role of Life Cycle Analyses from Building Designers’ Perspectives. *Energy Build.* **2015**, *108*, 463–469. [[CrossRef](#)]
53. Wang, B.; Xia, X.; Zhang, J. A Multi-Objective Optimization Model for the Life-Cycle Cost Analysis and Retrofitting Planning of Buildings. *Energy Build.* **2014**, *77*, 227–235. [[CrossRef](#)]
54. Cabeza, L.F.; Rincón, L.; Vilarinho, V.; Pérez, G.; Castell, A. Life Cycle Assessment (LCA) and Life Cycle Energy Analysis (LCEA) of Buildings and the Building Sector: A Review. *Renew. Sustain. Energy Rev.* **2014**, *29*, 394–416. [[CrossRef](#)]
55. Kneifel, J. Life-Cycle Carbon and Cost Analysis of Energy Efficiency Measures in New Commercial Buildings. *Energy Build.* **2010**, *42*, 333–340. [[CrossRef](#)]
56. Lee, W.L.; Yik, F.W.H.; Jones, P. A Strategy for Prioritising Interactive Measures for Enhancing Energy Efficiency of Air-Conditioned Buildings. *Energy* **2003**, *28*, 877–893. [[CrossRef](#)]
57. Zhou, Z.; Anwar, G.A.; Dong, Y. Performance-Based Bi-Objective Retrofit Optimization of Building Portfolios Considering Uncertainties and Environmental Impacts. *Buildings* **2022**, *12*, 85. [[CrossRef](#)]
58. Wang, M.; Cao, S.; Chen, D.; Ji, G.; Ma, Q.; Ren, Y. Research on Design Framework of Middle School Teaching Building Based on Performance Optimization and Prediction in the Scheme Design Stage. *Buildings* **2022**, *12*, 1897. [[CrossRef](#)]
59. Ghaderian, M.; Veysi, F. Multi-Objective Optimization of Energy Efficiency and Thermal Comfort in an Existing Office Building Using NSGA-II with Fitness Approximation: A Case Study. *J. Build. Eng.* **2021**, *41*, 102440. [[CrossRef](#)]
60. Abdou, N.; El Mghouchi, Y.; Hamdaoui, S.; El Asri, N.; Mouqallid, M. Multi-Objective Optimization of Passive Energy Efficiency Measures for Net-Zero Energy Building in Morocco. *Build. Environ.* **2021**, *204*, 108141. [[CrossRef](#)]
61. Chaturvedi, S.; Rajasekar, E.; Natarajan, S. Multi-Objective Building Design Optimization under Operational Uncertainties Using the NSGA II Algorithm. *Buildings* **2020**, *10*, 88. [[CrossRef](#)]
62. Si, B.; Wang, J.; Yao, X.; Shi, X.; Jin, X.; Zhou, X. Multi-Objective Optimization Design of a Complex Building Based on an Artificial Neural Network and Performance Evaluation of Algorithms. *Adv. Eng. Inform.* **2019**, *40*, 93–109. [[CrossRef](#)]
63. Harkouss, F.; Fardoun, F.; Biwole, P.H. Multi-Objective Optimization Methodology for Net Zero Energy Buildings. *J. Build. Eng.* **2018**, *16*, 57–71. [[CrossRef](#)]
64. Yue, N.; Caini, M.; Li, L.; Zhao, Y.; Li, Y. A Comparison of Six Metamodeling Techniques Applied to Multi Building Performance Vectors Prediction on Gymnasiums under Multiple Climate Conditions. *Appl. Energy* **2023**, *332*, 120481. [[CrossRef](#)]
65. Wu, D.-C.; Momeni, M.; Razban, A.; Chen, J. Optimizing Demand-Controlled Ventilation with Thermal Comfort and CO₂ Concentrations Using Long Short-Term Memory and Genetic Algorithm. *Build. Environ.* **2023**, *243*, 110676. [[CrossRef](#)]
66. Jędrzejczyk, A.; Firek, K.; Rusek, J. Convolutional Neural Network and Support Vector Machine for Prediction of Damage Intensity to Multi-Storey Prefabricated RC Buildings. *Energies* **2022**, *15*, 4736. [[CrossRef](#)]
67. Cordeiro-Costas, M.; Villanueva, D.; Eguía-Oller, P.; Granada-Álvarez, E. Machine Learning and Deep Learning Models Applied to Photovoltaic Production Forecasting. *Appl. Sci.* **2022**, *12*, 8769. [[CrossRef](#)]
68. Balachander, K.; Paulraj, D. Building Energy Time Series Data Mining for Behavior Analytics and Forecasting Energy Consumption. *KSII Trans. Internet Inf. Syst.* **2021**, *15*, 1957–1980. [[CrossRef](#)]
69. Wei, S.; Tien, P.W.; Wu, Y.; Calautit, J.K. The Impact of Deep Learning–Based Equipment Usage Detection on Building Energy Demand Estimation. *Build. Serv. Eng. Res. Technol.* **2021**, *42*, 545–557. [[CrossRef](#)]
70. Xu, F.; Liu, Q. Building Energy Consumption Optimization Method Based on Convolutional Neural Network and BIM. *Alex. Eng. J.* **2023**, *77*, 407–417. [[CrossRef](#)]

71. Wang, L.; Xie, D.; Zhou, L.; Zhang, Z. Application of the Hybrid Neural Network Model for Energy Consumption Prediction of Office Buildings. *J. Build. Eng.* **2023**, *72*, 106503. [[CrossRef](#)]
72. Peng, Y.; Shen, H.; Tang, X.; Zhang, S.; Zhao, J.; Liu, Y.; Nie, Y. Energy Consumption Optimization for Heating, Ventilation and Air Conditioning Systems Based on Deep Reinforcement Learning. *IEEE Access* **2023**, *11*, 88265–88277. [[CrossRef](#)]
73. Pal, R.; Tripathi, A.K.; Pandey, A.C.; Khan, M.A.; Menon, V.G.; Mittal, H. A N2CNN-Based Anomaly Detection Method for Cardiovascular Data in Cyber-Physical System. *IEEE Trans. Netw. Sci. Eng.* **2023**, *10*, 2617–2626. [[CrossRef](#)]
74. Jayashankara, M.; Shah, P.; Sharma, A.; Chanak, P.; Singh, S.K. A Novel Approach for Short-Term Energy Forecasting in Smart Buildings. *IEEE Sens. J.* **2023**, *23*, 5307–5314. [[CrossRef](#)]
75. Abida, A.; Richter, P. HVAC Control in Buildings Using Neural Network. *J. Build. Eng.* **2023**, *65*, 105558. [[CrossRef](#)]
76. Abdelaziz, A.; Santos, V.; Dias, M.S. Convolutional Neural Network with Genetic Algorithm for Predicting Energy Consumption in Public Buildings. *IEEE Access* **2023**, *11*, 64049–64069. [[CrossRef](#)]
77. Bakar, A.; Li, K.; Liu, H.; Xu, Z.; Alessandrini, M.; Wen, D. Multi-Objective Optimization of Low Reynolds Number Airfoil Using Convolutional Neural Network and Non-Dominated Sorting Genetic Algorithm. *Aerospace* **2022**, *9*, 35. [[CrossRef](#)]
78. Luo, X.J.; Oyedele, L.O. Life Cycle Optimisation of Building Retrofitting Considering Climate Change Effects. *Energy Build.* **2022**, *258*, 111830. [[CrossRef](#)]
79. Zhang, L.; Sang, G.; Zhu, Y.; Cui, X.; Han, W.; Zhang, Y.; Yu, H. Thermal Regulation Mechanism of Air-Drying Shelter to Indoor Environment of Earth Buildings Located in Turpan Basin with Extremely Dry and Hot Climate Conditions. *Sustain. Cities Soc.* **2023**, *91*, 104416. [[CrossRef](#)]
80. Evins, R. A Review of Computational Optimisation Methods Applied to Sustainable Building Design. *Renew. Sustain. Energy Rev.* **2013**, *22*, 230–245. [[CrossRef](#)]
81. Yang, J. Convergence and Uncertainty Analyses in Monte-Carlo Based Sensitivity Analysis. *Environ. Model. Softw.* **2011**, *26*, 444–457. [[CrossRef](#)]
82. Yamashita, R.; Nishio, M.; Do, R.K.G.; Togashi, K. Convolutional Neural Networks: An Overview and Application in Radiology. *Insights Imaging* **2018**, *9*, 611–629. [[CrossRef](#)] [[PubMed](#)]
83. Deb, K.; Pratap, A.; Agarwal, S.; Meyarivan, T. A Fast and Elitist Multiobjective Genetic Algorithm: NSGA-II. *IEEE Trans. Evol. Comput.* **2002**, *6*, 182–197. [[CrossRef](#)]
84. Zhu, S.; Liu, J.; Tang, G.; Sun, T.; Jia, H.; Zhao, H.; Zhang, Y.; Lin, L.; Xu, W. Evaluating the Application Potential of Acid-Modified Cotton Straw Biochars in Alkaline Soils Based on Entropy Weight TOPSIS. *Agronomy* **2023**, *13*, 2807. [[CrossRef](#)]
85. Moridi, S.S.; Moosavirad, S.H.; Mirhosseini, M.; Nikpour, H.; Mokhtari, A. Prioritizing power outages causes in different scenarios of the global business network matrix by using bwm and topsis. *Decis. Mak. Appl. Manag. Eng.* **2023**, *6*, 321–340. [[CrossRef](#)]
86. Liu, X.; Wang, W.; Wang, Z.; Song, J.; Li, K. Simulation Study on Outdoor Wind Environment of Residential Complexes in Hot-Summer and Cold-Winter Climate Zones Based on Entropy-Based TOPSIS Method. *Sustainability* **2023**, *15*, 12480. [[CrossRef](#)]
87. Zhao, C.; Chen, J.; Yang, X.; Yuan, J. Social and Economic Impact Assessment of Coal Power Phase-Down at the Provincial Level: An Entropy-Based TOPSIS Approach. *Sustainability* **2023**, *15*, 16175. [[CrossRef](#)]
88. Yuan, X.; Song, W. Evaluating Technology Innovation Capabilities of Companies Based on Entropy- TOPSIS: The Case of Solar Cell Companies. *Inf. Technol. Manag.* **2022**, *23*, 65–76. [[CrossRef](#)]
89. Xu, X.; Zhang, Z.; Long, T.; Sun, S.; Gao, J. Mega-City Region Sustainability Assessment and Obstacles Identification with GIS–Entropy–TOPSIS Model: A Case in Yangtze River Delta Urban Agglomeration, China. *J. Clean. Prod.* **2021**, *294*, 126147. [[CrossRef](#)]
90. Ding, S.; Li, R.; Guo, J. An Entropy-Based TOPSIS and Optimized Grey Prediction Model for Spatiotemporal Analysis in Strategic Emerging Industry. *Expert. Syst. Appl.* **2023**, *213*, 119169. [[CrossRef](#)]
91. Sun, J.; Miao, J.; Mu, H.; Xu, J.; Zhai, N. Sustainable Development in Marine Economy: Assessing Carrying Capacity of Shandong Province in China. *Ocean. Coast. Manag.* **2022**, *216*, 105981. [[CrossRef](#)]
92. Cao, J.; Xu, F. Entropy-Based Fuzzy TOPSIS Method for Investment Decision Optimization of Large-Scale Projects. *Comput. Intell. Neurosci.* **2022**, *2022*, e4381293. [[CrossRef](#)] [[PubMed](#)]
93. Nayak, P.P.; Datta, A.K. An Entropy-Based TOPSIS Approach for Selecting Best Suitable Rice Husk for Potential Energy Applications: Pyrolysis Kinetics and Characterization of Rice Husk and Rice Husk Ash. *Biomass Convers. Biorefin.* **2022**. [[CrossRef](#)]
94. Khavari, B.; Sahlberg, A.; Usher, W.; Korkovelos, A.; Nerini, F.F. Corrigendum to the Effects of Population Aggregation in Geospatial Electrification Planning [Energy Strategy Rev., 38 (2021), 100752]. *Energy Strategy Rev.* **2023**, *50*, 101262. [[CrossRef](#)]
95. Tissot, J.-Y.; Prieur, C. Bias Correction for the Estimation of Sensitivity Indices Based on Random Balance Designs. *Reliab. Eng. Syst. Saf.* **2012**, *107*, 205–213. [[CrossRef](#)]
96. Elbeltagi, E.; Wefki, H.; Abdrabou, S.; Dawood, M.; Ramzy, A. Visualized Strategy for Predicting Buildings Energy Consumption during Early Design Stage Using Parametric Analysis. *J. Build. Eng.* **2017**, *13*, 127–136. [[CrossRef](#)]
97. GB55015-2021; General Specification for Energy Efficiency and Renewable Energy Utilization in Buildings. Chinese Standard: Beijing, China, 2021.
98. Song, J.; Wang, W.; Ni, P.; Zheng, H.; Zhang, Z.; Zhou, Y. Framework on Low-Carbon Retrofit of Rural Residential Buildings in Arid Areas of Northwest China: A Case Study of Turpan Residential Buildings. *Build. Simul.* **2023**, *16*, 279–297. [[CrossRef](#)]
99. Xu, Y.; Zhou, Y.; Sekula, P.; Ding, L. Machine Learning in Construction: From Shallow to Deep Learning. *Dev. Built Environ.* **2021**, *6*, 100045. [[CrossRef](#)]

100. Guo, Y.; Xu, Y.; Li, S. Dense Construction Vehicle Detection Based on Orientation-Aware Feature Fusion Convolutional Neural Network. *Autom. Constr.* **2020**, *112*, 103124. [[CrossRef](#)]
101. Zhang, J.; Yang, X.; Li, W.; Zhang, S.; Jia, Y. Automatic Detection of Moisture Damages in Asphalt Pavements from GPR Data with Deep CNN and IRS Method. *Autom. Constr.* **2020**, *113*, 103119. [[CrossRef](#)]
102. Cai, M.; Pipattanasomporn, M.; Rahman, S. Day-Ahead Building-Level Load Forecasts Using Deep Learning vs. Traditional Time-Series Techniques. *Appl. Energy* **2019**, *236*, 1078–1088. [[CrossRef](#)]
103. Liu, S.; Ji, H.; Wang, M.C. Nonpooling Convolutional Neural Network Forecasting for Seasonal Time Series with Trends. *IEEE Trans. Neural Netw. Learn. Syst.* **2020**, *31*, 2879–2888. [[CrossRef](#)]
104. Liu, S.; Wang, Y.; Liu, X.; Yang, L.; Zhang, Y.; He, J. How Does Future Climatic Uncertainty Affect Multi-Objective Building Energy Retrofit Decisions? Evidence from Residential Buildings in Subtropical Hong Kong. *Sustain. Cities Soc.* **2023**, *92*, 104482. [[CrossRef](#)]
105. Yang, J.; Deng, Z.; Guo, S.; Chen, Y. Development of Bottom-up Model to Estimate Dynamic Carbon Emission for City-Scale Buildings. *Appl. Energy* **2023**, *331*, 120410. [[CrossRef](#)]
106. Luo, P.; Yu, B.; Li, P.; Liang, P.; Liang, Y.; Yang, L. How 2D and 3D Built Environments Impact Urban Surface Temperature under Extreme Heat: A Study in Chengdu, China. *Build. Environ.* **2023**, *231*, 110035. [[CrossRef](#)]
107. Gangoellis, M.; Gaspar, K.; Casals, M.; Ferré-Bigorra, J.; Forcada, N.; Macarulla, M. Life-Cycle Environmental and Cost-Effective Energy Retrofitting Solutions for Office Stock. *Sustain. Cities Soc.* **2020**, *61*, 102319. [[CrossRef](#)]
108. Feng, H.; Liyanage, D.R.; Karunathilake, H.; Sadiq, R.; Hewage, K. BIM-Based Life Cycle Environmental Performance Assessment of Single-Family Houses: Renovation and Reconstruction Strategies for Aging Building Stock in British Columbia. *J. Clean. Prod.* **2020**, *250*, 119543. [[CrossRef](#)]

Disclaimer/Publisher's Note: The statements, opinions and data contained in all publications are solely those of the individual author(s) and contributor(s) and not of MDPI and/or the editor(s). MDPI and/or the editor(s) disclaim responsibility for any injury to people or property resulting from any ideas, methods, instructions or products referred to in the content.